N73-33041

[redacted]

JET PROPULSION LABORATORY

CALIFORNIA INSTITUTE OF TECHNOLOGY

PASADENA, CALIFORNIA

72

900-636

PLANETARY QUARANTINE

Semi-Annual Review
Space Research and Technology

1 January - 30 June 1973

October, 1973

APPROVED BY:

D. M. Taylor, Supervisor
Life Sciences Research

A. R. Hoffman, Supervisor
Planetary Quarantine Analysis

D. S. Hess, Manager
Environmental Requirements
Section

JET PROPULSION LABORATORY
CALIFORNIA INSTITUTE OF TECHNOLOGY
PASADENA, CALIFORNIA

DISTRIBUTION

Caird, H.	111-118
Craven, C.	180-703
Flitton, D. D. (2)	111-208
Hess, D. S.	233-208
Hoffman, A. R. (2)	233-206
Small, J. G. (3)	180-703
Taylor, D. M. (75)	233-206

PREFACE

This document contains a report on Research and Advanced Development at the Jet Propulsion Laboratory during the period January, 1973 to July, 1973, sponsored by the Planetary Quarantine branch of the NASA Office of Space Science and Applications.

CONTENTS

I PLANETARY QUARANTINE STRATEGIES FOR ADVANCED MISSIONS (NASA No. 193-58-61-01) 1-1

1.1 STRATEGIES FOR SATELLITE ENCOUNTER 1-1

1.1.1 Subtask A Introduction 1-1

1.1.2 Significant Accomplishments 1-1

1.1.3 Future Activities 1-1

1.1.4 Presentations 1-1

1.2 JUPITER ENTRY ANALYSIS 1-2

1.2.1 Subtask B Introduction 1-2

1.2.2 Significant Accomplishments 1-2

1.2.3 Future Activities 1-2

1.2.4 Presentations 1-3

II NATURAL SPACE ENVIRONMENT STUDIES (NASA No. 193-58-61-02) 2-1

2.1 EFFECT OF PLANETARY TRAPPED RADIATION BELT ON MICROORGANISMS 2-1

2.1.1 Subtask A Introduction 2-1

2.1.2 Significant Accomplishments 2-1

2.1.3 Future Activities 2-9

2.2 EFFECT OF SOLAR WIND RADIATION ON MICROORGANISMS 2-10

2.2.1 Subtask B Introduction 2-10

2.2.2 Significant Accomplishments 2-10

2.2.3 Future Activities 2-10

2.3 EFFECT OF SPACE VACUUM ON MICROORGANISMS 2-11

2.3.1 Subtask C Introduction 2-11

2.3.2 Significant Accomplishments 2-11

2.3.3 Future Activities 2-13

2.3.4 Presentations 2-14

III POST LAUNCH RECONTAMINATION STUDIES (NASA No. 193-58-62-03) 3-1

3.1 POST LAUNCH RECONTAMINATION STUDIES 3-1

3.1.1 Subtask A Introduction 3-1

3.1.2 Significant Accomplishments 3-1

CONTENTS (contd)

3.1.3 Future Activities 3-14
3.1.4 Presentations 3-16
3.1.5 Publications 3-16
3.1.6 References 3-16

IV SPACECRAFT CLEANING AND DECONTAMINATION TECHNIQUES (NASA No. 193-58-63-02) 4-1

4.1 PHYSICAL REMOVAL OF SPACECRAFT MICROBIAL BURDEN 4-1
4.1.1 Subtask A Introduction 4-1
4.1.2 Approach 4-1
4.1.3 Significant Accomplishments 4-6
4.1.4 Summary and Conclusions 4-17
4.1.5 Future Activities 4-19

4.2 EVALUATION OF PLASMA CLEANING AND DECONTAMINATION TECHNIQUES 4-21
4.2.1 Subtask B Introduction 4-21
4.2.2 Significant Accomplishments 4-21
4.2.3 Future Activities 4-21

FIGURES

2-A.1	Effect of dose and dose rate at different electron energies on spacecraft spore isolates	2-5
2-A.2	Effect of dose and dose rate at different electron energies on spacecraft nonsporeformer isolates	2-7
2-A.3	Response of bacterial spores to 2 MeV electron and proton irradiation	2-8
2-C.1	Effect of temperature on combined spacecraft isolates in vacuum (Vegetatives)	2-15
2-C.2	Effect of temperature on combined spacecraft isolates in vacuum (Spores)	2-15
2-C.3	Effect of vacuum duration on combined spacecraft isolates (Vegetatives)	2-16
2-C.4	Effect of vacuum duration on combined spacecraft isolates (Spores)	2-16
2-C.5	Interaction of vacuum duration and temperature on combined spacecraft isolates (Vegetatives)	2-17
2-C.6	Interaction of vacuum duration and temperature on combined spacecraft isolates (Spores)	2-18
2-C.7	Summary of vacuum-temperature studies (Vegetatives)	2-19
2-C.8	Summary of vacuum-temperature studies (Spores)	2-20
3-A.1	Particle adhesion experimental apparatus	3-1
3-A.2	Meteoroid impact analysis results (case I)	3-6
3-A.3	Meteoroid impact analysis results (case II)	3-6
3-A.4	One dimensional electric field	3-9
3-A.5	Grain charging in sunlight	3-11
3-A.6	Particle trajectory calculations	3-12
3-A.7	Conceptual schematic for acoustic emission application to particle release	3-14
3-A.8	Flow diagram for spacecraft recontamination analysis	3-15
4-A.1	Typical size distribution of glass beads used for test	4-3
4-A.2	Test apparatus (as seen in schematic, Fig. 4-A.3)	4-4
4-A.3	Apparatus schematic	4-5
4-A.4	Removal efficiency vs blow angle and pressure	4-6
4-A.5	Removal efficiency vs blow-pressure for different surface conditions (45 deg blow angle)	4-7
4-A.6	Efficiency gain vs sweep pattern	4-9

FIGURES (contd)

4-A.7 Efficiency gain vs number of strokes 4-11

4-A.8 Tests with dust --total removal efficiencies vs pressure and surface conditions (45 deg blow angle, double sweep) 4-13

4-A.9 Tests with dust on dry surface; effect on size (45 deg blow) 4-14

4-A.10 Tests with dust on oily surface; effect on size (45 deg blow). . . . 4-15

4-A.11 Test with dust on moistened surface; effect on size (45 deg blow) . 4-16

TABLES

2-A.1 Conversion for Electron Tests 2-3

2-A.2 Conversion for Proton Tests 2-3

2-A.3 Percent Survival of Spores Exposed to Electron Irradiation 2-4

2-A.4 Percent Survival of Nonsporeformers Exposed to Electron Irradiation 2-6

2-A.5 Percent survival of Spacecraft Isolates Exposed to 2 MeV Proton Irradiation 2-8

3-A.1 Particle Adhesion Test Results 3-4

4-A.1 Blow vacuum cleaning test efficiencies demonstrated with dust seeded on optical glass 4-17

SECTION I

PLANETARY QUARANTINE STRATEGIES FOR ADVANCED MISSIONS (NASA No. 193-58-61-01)

Contents

Subtask A para. 1.1 — STRATEGIES FOR SATELLITE ENCOUNTER

Cognizance: C. Gonzalez

Associate Personnel: W. Stavro

Subtask B para. 1.2 — JUPITER ENTRY ANALYSIS

Cognizance: C. Gonzalez

Associate Personnel: W. Jaworski, A. McRonald

1.1 STRATEGIES FOR SATELLITE ENCOUNTER

1.1.1 Subtask A Introduction

The objectives of this task are to determine the impact of satisfying satellite quarantine constraints on current outer planet mission and spacecraft designs; and to develop tools required to perform trajectory and navigation analyses for determining satellite impact probabilities.

1.1.2 Significant Accomplishments

Previously developed software tools were applied to typical outer planet close satellite encounters involving Io (Jupiter) and Titan (Saturn). The probability of impact of the satellite by a spacecraft was determined for various midcourse maneuvers. The implications for outer planet missions of satisfying satellite quarantine constraints were determined. The results of the satellite quarantine analyses were presented at the COSPAR meeting (June 1973) in Germany, and at the AIAA/AGU meeting on the outer planets (July 1973) in Denver.

The probability of impacting Saturn's rings was also determined.

1.1.3 Future Activities

The following future activities will be undertaken:

1) A calculation of the probability of impact for Ganymede (Jupiter) and Tethys (Saturn) encounters.

2) A determination of the implications of a JS - X mission on satellite and planetary quarantine.

3) A determination of any fuel load penalties which would be required to satisfy the quarantine constraints.

4) An investigation of strategies to minimize the fuel load penalties.

1.1.4 Presentations

Hoffman, A. R., Stavro, W., Gonzales, C., "Quarantine Constraints as Applied to Satellites." Paper presented at the Joint Open Meeting of the

Panel on Planetary Quarantine at the 16th Meeting of COSPAR, Konstanz, F. R. G., May 25 – June 6, 1973.

Gonzalez, C., Stavro, W., "The Significance of Outer Planet Satellite Quarantine Constraints on Aim-Point Selection." Paper presented at the AIAA/AGU Space Science Conference on the Exploration of the Outer Solar System, Denver, Colorado, July 10-12, 1973.

1.2 JUPITER ENTRY ANALYSIS

1.2.1 Subtask B Introduction

The objective of the task is to develop and use tools needed to determine the thermal response characteristics of a typical spacecraft and related debris upon entry into the Jovian atmosphere.

1.2.2 Significant Accomplishments

A thermal response analysis was performed for the ultraviolet spectrometer (UVS) lens cap and indicated that components, such as the lens cap which are comprised of a homogeneous material (e.g., plastic) and are small in size (23.0 cm in diameter, 24.0 cm long and 0.5 cm thick), will not survive atmospheric entry. Thermal modeling of the UVS itself was initiated and is still in progress at the writing of this report. The chemical and thermal properties of the UVS component materials have been determined.

The particle analyses for Jupiter are nearly completed.

1.2.3 Future Activities

Future activities for the next six months include completion of all particle analyses for Jupiter, and initiation of similar analyses for Saturn. Thermal modeling will be completed for the UVS and an entry heating analysis performed. Thermal modeling will also be completed for the spacecraft mission module.

1.2.4 Presentations

Gonzalez, C., Jaworski, W., McRonald, A., and Hoffman, A., "Spacecraft Microbial Burden Reduction Due to Atmospheric Entry Heating – Jupiter." Paper presented at the Joint Open Meeting of the Panel on Planetary Quarantine at the 16th Meeting of COSPAR, Konstanz, F. R. G., May 25 – June 6, 1973.

SECTION II

NATURAL SPACE ENVIRONMENT STUDIES
(NASA No. 193-58-61-02)

Contents	Title and Related Personnel
Subtask A para. 2.1	EFFECT OF PLANETARY TRAPPED RADIATION BELT ON MICROORGANISMS Cognizance: D. Taylor Associate Personnel: C. Hagen (Bionetics) J. Barengoltz C. Smith (Bionetics) G. Renninger (Bionetics)
Subtask B para. 2.2	EFFECT OF SOLAR WIND ON MICROORGANISMS Cognizance: D. Taylor Associate Personnel: C. Hagen (Bionetics) J. Barengoltz
Subtask C para. 2.3	EFFECT OF SPACE VACUUM ON MICROORGANISMS Cognizance: D. Taylor C. Hagen (Bionetics) Associate Personnel: R. Gildersleeve (Bionetics) G. Simko (Bionetics) J. Yelinek (Bionetics) C. Smith (Bionetics)

2.1 EFFECT OF PLANETARY TRAPPED RADIATION BELT ON MICROORGANISMS

2.1.1 Subtask A Introduction

The objective of this subtask is to determine the effect of planetary trapped radiation belts on the survival of microorganisms associated with an unsterile spacecraft.

With flyby missions now planned for Jupiter and Saturn and possible Jupiter orbiters and probes, the trapped radiation belts may represent an environment lethal to microorganisms and thereby reduce the requirement for decontamination of spacecraft before launch.

The major components of planetary trapped radiation belts are electrons and protons. The approach of the present task is to evaluate possible biological effects of these belts by subjecting spacecraft microbial isolates to different energies, exposures, and dose rates of those particles.

2.1.2 Significant Accomplishments

2.1.2.1 Description of Study. During this reporting period a test matrix for 2, 12, and 25 MeV electron exposures was completed. Additional 2 MeV proton exposures other than those previously reported (JPL Doc. No. 900-608, 1 July-31 December 1972) were completed.

As with all the radiation studies, a spacecraft bacterial subpopulation (nine sporeforming and three nonsporeforming isolates) plus two comparative organisms, Staphylococcus epidermidis and spores of Bacillus subtilis var. niger, were exposed to the different particle radiations at different exposures and exposure rates with simultaneous exposure to a vacuum of 10^{-6} torr at -20 and 20°C.

2.1.2.2 Experimental Conditions.

1. Microbiology. The derivation, culture, and assay procedures for the test organisms were previously described in para. 3.2.1.2 of JPL Doc. No. 900-597, February 1973.

2. Vacuum Equipment. Photographs, together with a description of the test facility, were presented in para. 3.2.3.4 of JPL Doc. No. 900-484, 1 July-31 December 1970.

3. Radiation Equipment. The 2 MeV electrons were produced by a dynamitron, a direct current accelerator. The flux profile was established and the exposure was monitored with the use of Faraday cups. The 12 and 25 MeV electrons were produced by a LINAC operated at 15 pulses sec^{-1} and a pulse width of 2 to 3 μsec. The absolute fluence per pulse was established prior to each run with LiF thermoluminescent detectors (TLD). The magnitude and number of the pulses in these maps and during the test runs was standardized by a center mounted PIN diode.

The bacterial isolates were exposed to 2, 12, and 25 MeV electrons, at 150, 300, and 450 krad with dose rates of 30, 300, and 3,000 rad sec^{-1}.

The 2 MeV protons were produced by a dynamitron with the isolates exposed to 1,350, 2,700, and 13,500 krad with a dose rate of 2,700 rad sec^{-1}. Additional exposures were conducted with the same proton energy with a dose of 2,700 krad with dose rates of 270 and 108,000 rad sec^{-1}.

Since the current model of the trapped radiation belt of Jupiter is given in terms of flux and energy, Tables 2-A.1 and 2-A.2 present conversion data for dose (krad) to fluence (particles cm^{-2}) and dose rate (rad sec^{-1}) to flux (particles $cm^{-2}sec^{-1}$) for electrons and protons.

As shown in Table 2-A.1 the highest dose rate with both 12 and 25 MeV electrons was lower than the highest dose rate with the 2 MeV electrons. This was the result of limitations in source capability.

2.1.2.3 Results. The percent survival of spores exposed to electron irradiation is shown in Table 2-A.3. In all of the reported data the geometric mean percent survival was based on data obtained from replication of each test condition four times. In addition, the data obtained from each single replication was based on a geometric mean percent survival obtained from three plate counts.

Table 2-A. 1. Conversion for Electron Tests

ENERGY, MeV		FLUX, $cm^{-2}\ sec^{-1}$	DOSE RATE, $rad\ sec^{-1}$	FLUENCE, cm^{-2}	DOSE, krad	
NOMINAL	ACTUAL				NOMINAL	ACTUAL
2	1.93	10^9	30	4.85×10^{12}	150	145
		10^{10}	300	9.70×10^{12}	300	290
		10^{11}	3000	1.45×10^{13}	450	440
12	10.65	8.4×10^8	30	4.10×10^{12}	150	145
		8.4×10^9	300	8.20×10^{12}	300	290
		6.5×10^{10}	2200	1.24×10^{13}	450	440
25	23.40	7.0×10^8	30	3.50×10^{12}	150	145
		7.1×10^9	300	7.00×10^{12}	300	290
		5.4×10^{10}	2200	1.07×10^{13}	450	440

Table 2-A. 2. Conversion for Proton Tests

ENERGY, MeV	Flux $cm^{-2}\ sec^{-1}$	Dose Rate $rad\ sec^{-1}$	Fluence cm^{-2}	Dose Krad
2	10^8	270	5×10^{11}	1350
	10^9	2700	1×10^{12}	2700
	4×10^{10}	108000	5×10^{12}	13500

Table 2-A. 3. Percent Survival of Spores Exposed to Electron Irradiation

	ENERGY, MeV								
	2			12			25		
	DOSE RATE, rad sec^{-1}			DOSE RATE, rad sec^{-1}			DOSE RATE, rad sec^{-1}		
DOSE, Krad	30	300	3000	30	300	2200	30	300	2200
150	21.4[1] (11.73)[2]	11.40 (7.62)	16.17 (10.81)	34.46 (25.83)	28.42 (23.60)	33.50 (16.91)	27.64 (30.02)	29.12 (23.71)	22.37 (14.92)
300	1.32 (0.53)	0.77 (0.37)	1.00 (0.40)	8.92 (6.27)	6.10 (3.92)	8.78 (6.23)	16.84 (12.41)	15.26 (5.96)	12.87 (8.19)
450	0.50 (0.12)	0.07 (0.03)	0.42 (0.06)	1.26 (0.54)	2.77 (1.12)	1.08 (0.27)	2.40 (0.91)	5.16 (3.44)	1.83 (0.45)

[1] MEAN OF SPACECRAFT ISOLATES

[2] B. subtilis

As shown in Table 2-A. 3 spores of the comparative organism, B. subtilis (survival fractions in parenthesis), were less radioresistant than the mean of spores of the spacecraft isolates. An approximate one log reduction occurred for each 150 krad dose with the 2 MeV electrons. At the higher electron energies of 12 and 25 MeV the dose response was less. An increase in dose rate from 30 to 300 and finally to 3,000 rad sec^{-1} had a less pronounced effect on the percent survival of spores than the dose effect. An interaction of dose rate and electron energy also occurred with the 2 MeV electrons being the most effective of the three electron energies studied.

Figure 2-A. 1 shows the subtle relationships existing between dose and dose rate at the different electron energies on the survival of spores of spacecraft isolates. With 2 MeV electrons a dose of 450 krad at 300 rad sec^{-1} dose rate was the most effective. Greater survival fractions occurred at both 30 and 3,000 rad sec^{-1} dose rates for 450 krad. With increased

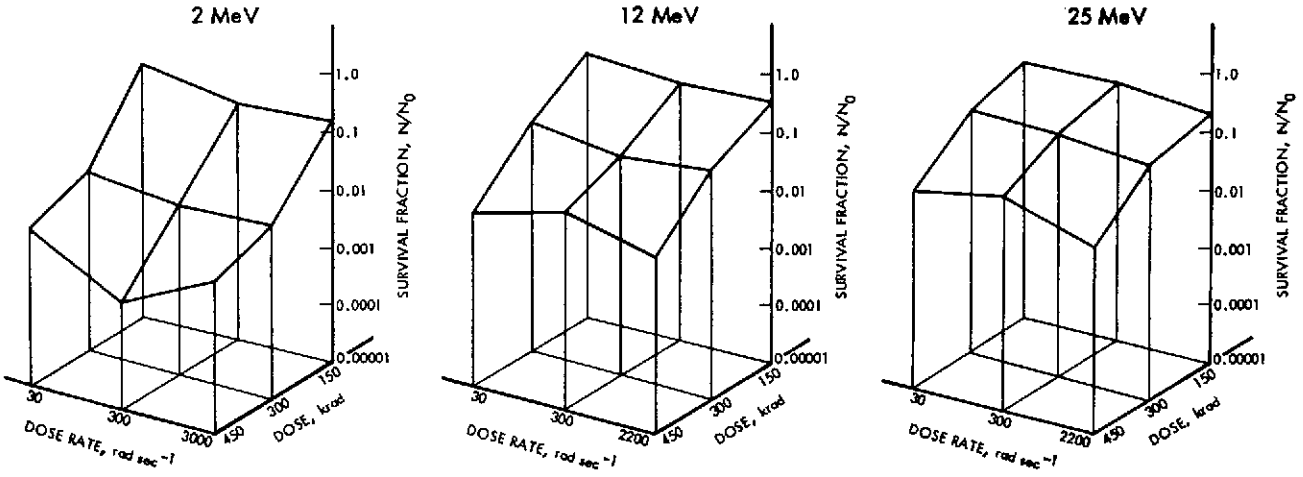

Fig. 2-A.1. Effect of dose and dose rate at different electron energies on spacecraft spore isolates

electron energy to 12 and 25 MeV a dose of 450 krad at both dose rates of 30 and 2,200 rad sec^{-1} became the most effective. This is shown as a downturning of the projected planes in Fig. 2-A.1 for the 12 and 25 MeV electrons.

The percent survival of nonsporeformers exposed to electron irradiation is shown in Table 2-A.4. The comparative organism, S. epidermidis, was considerably less radioresistant than the mean of the nonsporeforming spacecraft isolates.

The overall radioresistance of the nonsporeforming isolates to the different electron radiation environments was less than the spores of the sporeforming isolates. Also, with the nonsporeforming isolates there was less of an electron energy effect compared to the spores. The 12 MeV electron energy was slightly more effective, particularly at the higher exposures, than either the 2 or 25 MeV electron energies on the survival of the nonsporeforming isolates.

Table 2-A. 4. Percent Survival of Nonsporeformers Exposed to Electron Irradiation

EXPOSURE, Krad	ENERGY, MeV								
	2			12			25		
	DOSE RATE, rad sec^{-1}			DOSE RATE, rad sec^{-1}			DOSE RATE, rad sec^{-1}		
	30	300	3000	30	300	2200	30	300	2200
150	2.21[1] (0.77)[2]	9.31 (1.03)	2.14 (0.006)	8.37 (0.56)	7.45 (1.22)	4.92 (2.97)	9.37 (1.18)	9.24 (4.04)	0.79 (0.18)
300	0.31 (0.003)	0.34 (0.0003)	0.20 (0.00002)	0.41 (0.42)	0.04 (0.0004)	0.008 (0.00003)	2.60 (0.07)	0.48 (0.07)	0.05 (0.003)
450	0.001 (0.00002)	0.006 (0.00004)	0.0004 (0.00001)	0.0002 (0.00002)	0.001 (0.00001)	0.0002 (0.00001)	0.01 (0.0004)	0.15 (0.02)	0.0002 (0.00001)

[1]MEAN OF SPACECRAFT ISOLATES
[2]S. epidermidis

The effect of exposure was greater with the nonsporeforming isolates than with the spores. Initial populations of nonsporeforming isolates were reduced, in general, between 1.5 to 2.0 logs for each 150 krad exposure.

The data from Table 2-A.4 is represented as projected planes in Fig. 2-A.2 to show the relationships between dose, dose rate, and electron energy. In contrast to the dose rate effect found with spores at 2 MeV, the 300 rad sec^{-1} dose rate generally was less effective than the other dose rates at all energies studied with nonsporeforming isolates. This is shown in Fig. 2-A.2 as a downturning of the planes for all electron energies, particularly with the 450 krad dose at dose rates of 30 and 3,000 (2,200) rad sec^{-1}.

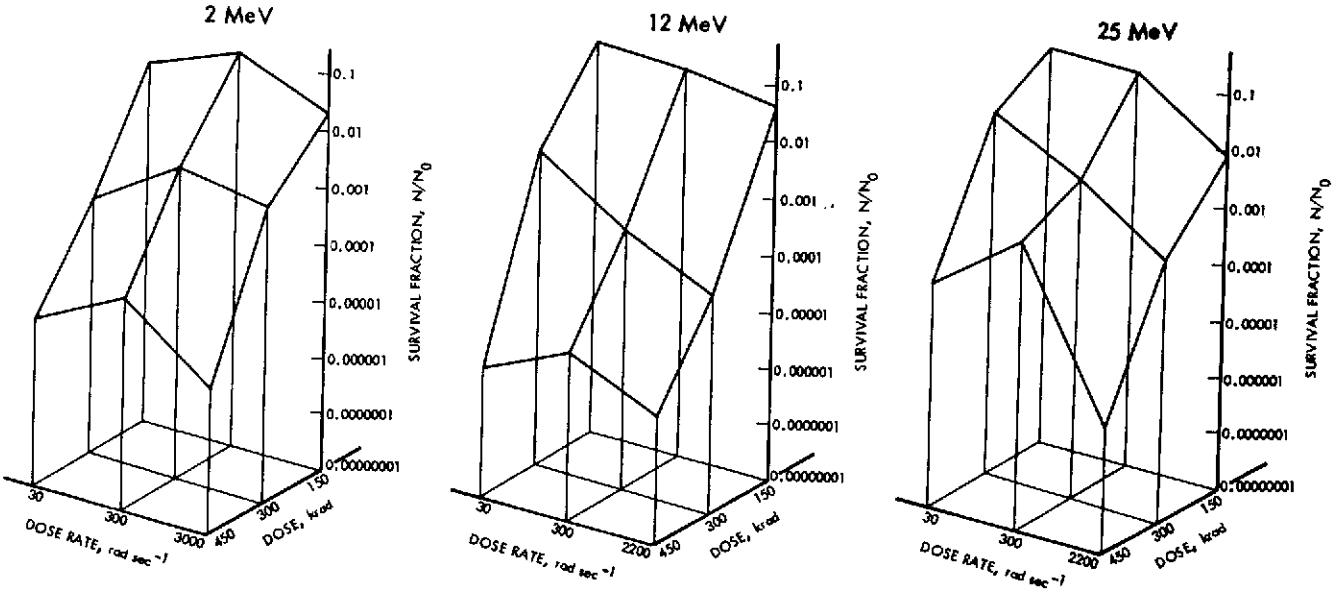

Fig. 2-A.2. Effect of dose and dose rate at different electron energies on spacecraft nonsporeformer isolates

Also shown in Fig. 2-A.2 is that with increasing dose and electron energy smaller survival fractions of the nonsporeforming isolates resulted.

The results from 2 MeV proton irradiation of spores and nonsporeformers are shown in Table 2-A.5. Both spores and nonsporeformers reacted in a similar manner to dose rate with the 2 MeV protons. At a constant dose of 2,700 krad the lower dose rates of 270 and 2,700 rad sec^{-1} were more effective than the highest dose rate studied, 108,000 rad sec^{-1}.

The exposure, or dose, effect was different with spores and nonsporeformers. The radiosensitivity of the spores increased as the exposure increased with a constant dose rate of 2,700 rad sec^{-1}. With the nonsporeformers the high dose, 13,500 krad, was the most effective with a constant dose rate of 2,700 rad sec^{-1}. Percent survival with 1,350 and 2,700 krad was approximately the same.

Fig. 2-A.3 shows the response of bacterial spores to 2 MeV electron electron and proton irradiation on a fluence basis. The comparative organism, B. subtilis, was more sensitive than the spores of the spacecraft isolates to both types of irradiation at all fluences. Also, it appeared

Table 2-A. 5. Percent survival of Spacecraft Isolates Exposed to 2 MeV Proton Irradiation

DOSE, krad		DOSE RATE, rad sec^{-1}		
		270	2700	108,000
SPORES	1350		17.8 (12.3)	
	2700	11.7[1] (9.2)[2]	10.4 (9.4)	29.0 (27.4)
	13500		4.3 (1.9)	
NONSPOREFORMERS	1350		0.0179 (0.0938)	
	2700	0.0035[3] (0.0046)[4]	0.0361 (0.0087)	3.54 (0.125)
	13500		0.0015 (0.0002)	

[1]MEAN OF SPACECRAFT SPORE ISOLATES [3]MEAN OF SPACECRAFT NONSPOREFORMER ISOLATES

[2]B. subtilis [4]S. epidermidis

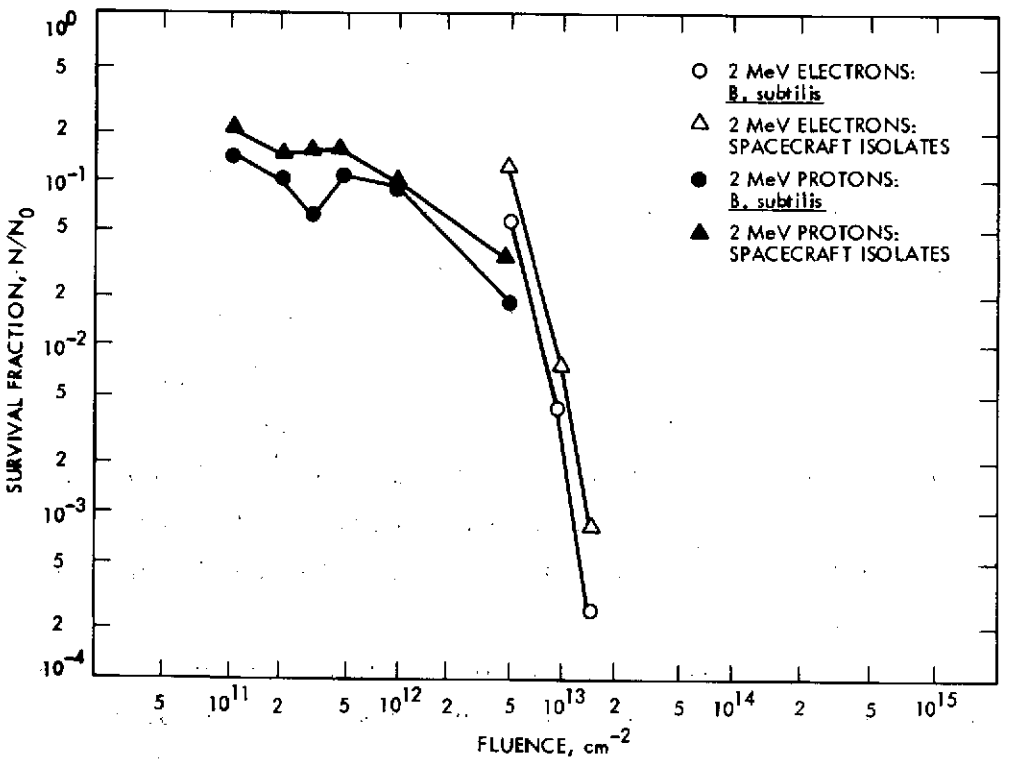

Fig. 2-A. 3. Response of bacterial spores to 2 MeV electron and proton irradiation

that the proton irradiation may be more effective than electron irradiation but additional work will have to be conducted before final conclusions can be reached. A proton fluence of 10^{12} cm^{-2} yielded survival fractions comparable to an electron fluence of 5×10^{12} cm^{-2} and a proton fluence of 5×10^{12} cm^{-2} resulted in survival fractions lower than the same electron fluence.

In summary, the results from electron irradiation tests at this time indicate that energy and dose are the most effective parameters. The initial populations of nonsporeformers were reduced at least 90 percent at all energies and doses studied. The spores were reduced at least 90 percent at 300 and 450 krad with 2 and 12 MeV energies and at 450 krad with 25 MeV. There were also indications that dose rate could become an important parameter under conditions of high exposures, or doses.

2.1.3 Future Activities

Future activities in these studies to determine the effect of planetary trapped radiation belt on microorganisms will be to complete the 0.6 MeV electron tests; to investigate the effect of 12 and 25 MeV protons; to evaluate the effect of secondary radiations on microbial survival; and, finally, to analyze and model the radiation sensitivity of microbial populations.

2.2 EFFECT OF SOLAR WIND RADIATION ON MICROORGANISMS

2.2.1 Subtask B Introduction

The objective of this subtask is to determine the effect of solar wind radiation on microorganisms associated with nonsterile spacecraft.

This study is directed towards determining the reduction in spacecraft associated microbial burden attributable to solar wind radiation.

The approach does not attempt a simulation of the total radiation environment, but rather to examine the effect of low energy electrons and protons as a function of dose and energy. The data acquired would apply to all missions.

2.2.2 Significant Accomplishments

Due to reprogramming of resources the level of effort on this task had to be reduced. The study will be conducted in-house so that the schedule can be adjusted in accordance with resources available. An experimental setup has been designed and preliminary tests are underway to determine the effect of 100 eV electrons on bacterial isolates.

2.2.3 Future Activities

Complete a preliminary experiment with 100 eV electrons. Conduct a low energy electron study at three energies, exposures, and dose rates. Design or locate an existing facility to conduct an analogous test program for low energy protons.

2.3 EFFECT OF SPACE VACUUM ON MICROORGANISMS

2.3.1 Subtask C Introduction

This study was designed to examine the combined effects of space vacuum and spacecraft temperatures on the survival of microorganisms. Fourteen isolates were exposed to the test conditions. Nine of the isolates, recovered from MM'71 spacecraft, were sporeformers while three isolates were nonsporeformers. A sporeforming organism, Bacillus subtilis var. niger, and a nonsporeforming organism, Staphylococcus epidermidis ATCC 17917, were included in the tests for comparative purposes.

A vacuum exposure (10^{-8} torr) of the bacterial isolates to temperatures of -40, 25, 40, and 55°C were conducted for 7, 14, 28, 56, and 187 days to simulate the vacuum and temperature environment of a spacecraft during typical mission to Mars.

This study has been reported in earlier reports and only the results of the final analysis of the data is reported here.

2.3.2 Significant Accomplishments

2.3.2.1 Experimental Conditions.

1. Microbiology. The test organisms, isolated from MM'71 spacecraft, were the same organisms that were used in the launch pressure profile study and are presently being used in the space radiation study. The derivation, culture, and assay procedures for the isolates are described in para 3.2.1.2 of the Annual Report (JPL Doc. No. 900-597, February, 1973).

2. Vacuum Equipment. Photographs, together with a description of the test facility, are presented in para. 3.2.1.2 of the Annual Report (JPL Doc. No. 900-597, February, 1973).

2.3.2.2 Results. The effects of temperature at 25, 40, and 55°C on the nonsporeforming spacecraft isolates held in vacuum are shown in Fig. 2-C.1. Survival data from exposure to -40°C are not presented because survival fractions were still greater than 0.1 after the 187-day exposure.

There is a zone of uncertainty that with the nonsporeforming isolates that occurred up to 56 days of vacuum-temperature exposure and is represented as troughs in the survivor curves for 25, 40, and 55° C. When the temperature was increased from 25°C to 55°C the trough effect lessened. The implication is cell membrane injury with subsequent recovery, or repair, as the vacuum-temperature exposure time is increased. However, this effect is overcome with increased temperatures at 40 and 55°C, that are known to impair the cell's membrane integrity.

The trough phenomenon occurred to a lesser extent with the spores of spacecraft isolates, Fig. 2-C.2. The trough effect occurred up to 28 days only at 25 and 40°C.

Temperature effect with vacuum exposure for nonsporeforming spacecraft isolates is shown in Fig. 2-C.3. During 28 days vacuum exposure a slow die-off of the cells occurred possibly as a result of desiccation, with or without, combined temperature effect. A true temperature effect was manifested between 40 and 55°C. After 56- and 187-day exposures the temperature effect was displaced to between 25 and 40°C.

The effect of temperature on vacuum survival of spores of spacecraft isolates is shown in Fig. 2-C.4. It appeared that the critical temperature was between 25 and 40°C and that the temperature effect occurred as early as 28 days.

The combined effect of temperature and duration of vacuum exposure on nonsporeforming spacecraft isolates is shown in Fig. 2-C.5. The trough effect mentioned earlier was quite noticeable with the three dimensional plot and occurred to some extent at all temperatures up to 56 days. The least pronounced trough effect was observed at 55° C.

The combined effect of temperature and duration of vacuum exposure on spores of spacecraft isolates is shown in Fig. 2-C.6. The trough effect occurred between 14 and 28 days and was temperature dependent with no trough effect occurring at 55° C and the greatest at -40° C.

Figure 2-C.7 summarizes survival data for temperatures of -40, 25, 40, and 55°C with 28-, 56-, and 187-day vacuum exposures for nonsporeforming spacecraft isolates. Although a critical temperature effect between 25 and

40° C was not pronounced with the 28-day exposure, it was quite pronounced with both the 56-day and 187-day vacuum exposures.

Summary data for spores of spacecraft isolates showing the temperature effect as a function of vacuum exposure duration is presented in Fig. 2-C.8. At the 28-, 56-, and 187-day vacuum exposures a temperature effect became noticeable between 25 and 40° C with a pronounced effect occurring between 40 and 55° C.

In summary:

1) The effect of space vacuum in conjunction with normal operating temperatures of spacecraft on the survival of spacecraft isolates was found to be highly dependent upon the duration of vacuum exposure, temperature, and the individual isolate;
2) Temperatures of -40 and 25° C did not effectively reduce initial populations even after an 187-day exposure;
3) Temperatures of 40 and 55° C, while effective in reducing initial populations, did permit survival after as long as an 187-day exposure;
4) After an 187-day vacuum exposure survival fractions of spacecraft isolate spores were 1.77, 0.67, 0.04, and 0.002 with temperatures of -40, 25, 40, and 55° C, respectively;
5) After an 187-day vacuum exposure, survival fractions of non-sporeforming spacecraft isolates were 0.33, 0.07, 0.02 and 0.003 for temperatures of -40, 25, 40, and 55° C, respectively.

2.3.3 Future Activities

Future activities of the vacuum temperature will be to initiate studies to investigate the thermal vacuum resistance of naturally occurring (uncultured) organisms. In addition, the fact that VO'75 spacecraft may experience higher temperatures for longer periods of time than MM'71 spacecraft may indicate the need for future studies of vacuum exposures with higher temperatures than thos reported in the present study.

2.3.4 Presentations

Taylor, D. M., "Effect of Space Vacuum on Microorganisms," presented to the AIBS Planetary Quarantine Panel, Cocoa Beach, Florida, April 26, 1973.

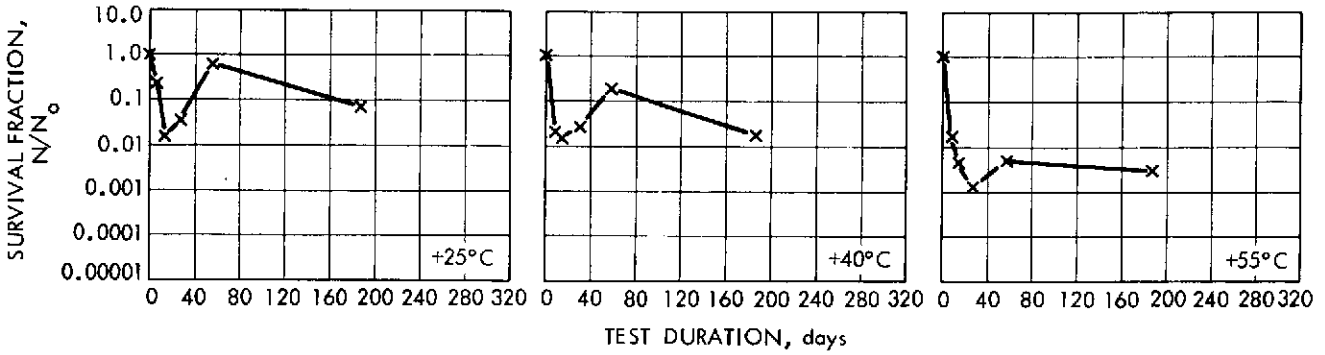

Fig. 2-C.1. Effect of temperature on combined spacecraft isolates in vacuum (Vegetatives)

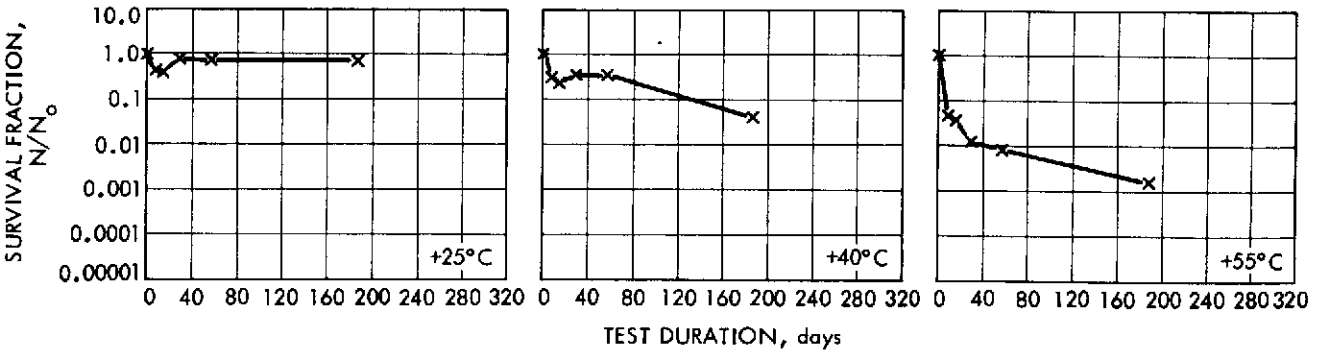

Fig. 2-C.2. Effect of temperature on combined spacecraft isolates in vacuum (Spores)

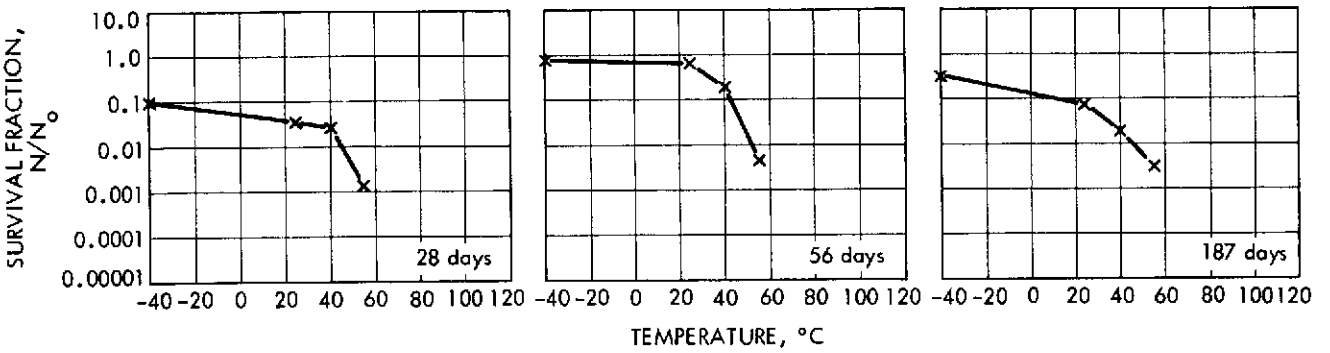

Fig. 2-C.3. Effect of vacuum duration on combined spacecraft isolates (Vegetatives)

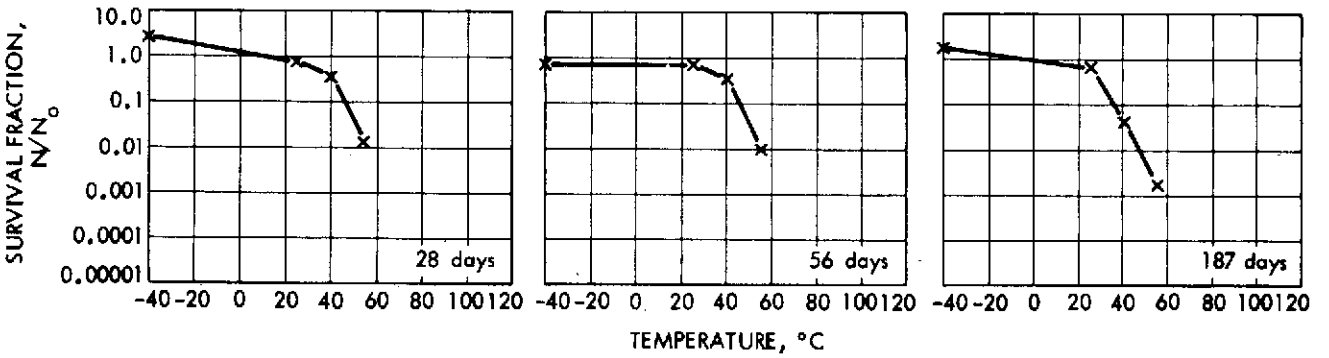

Fig. 2-C.4. Effect of vacuum duration on combined spacecraft isolates (Spores)

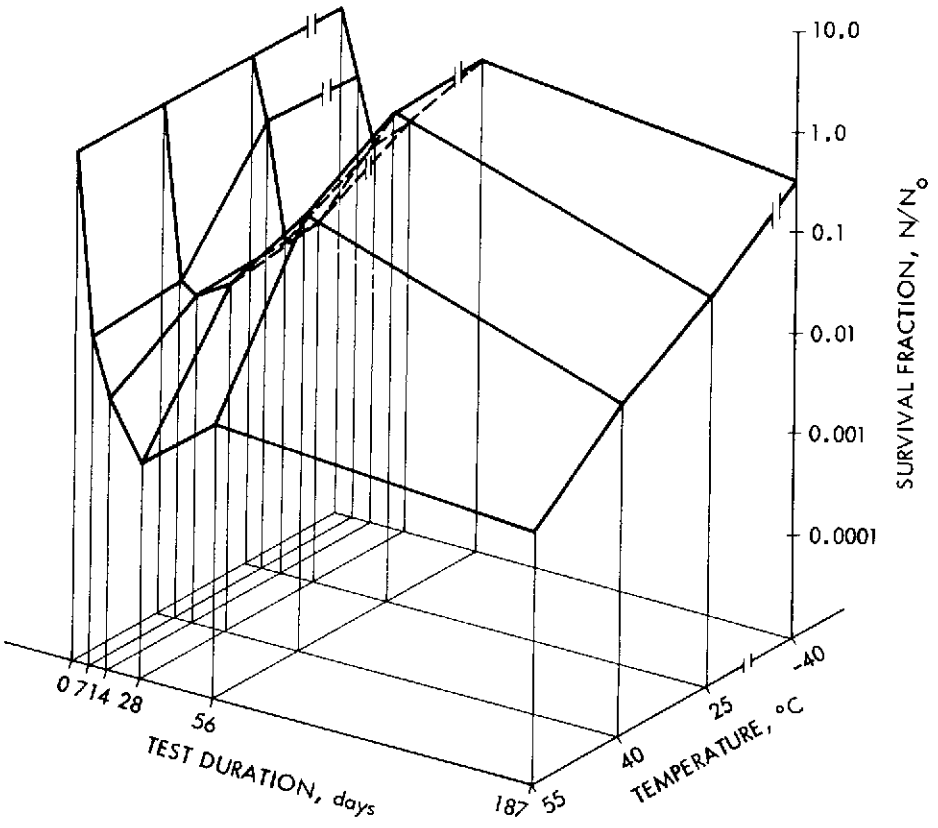

Fig. 2-C.5. Interaction of vacuum duration and temperature on combined spacecraft isolates (Vegetatives)

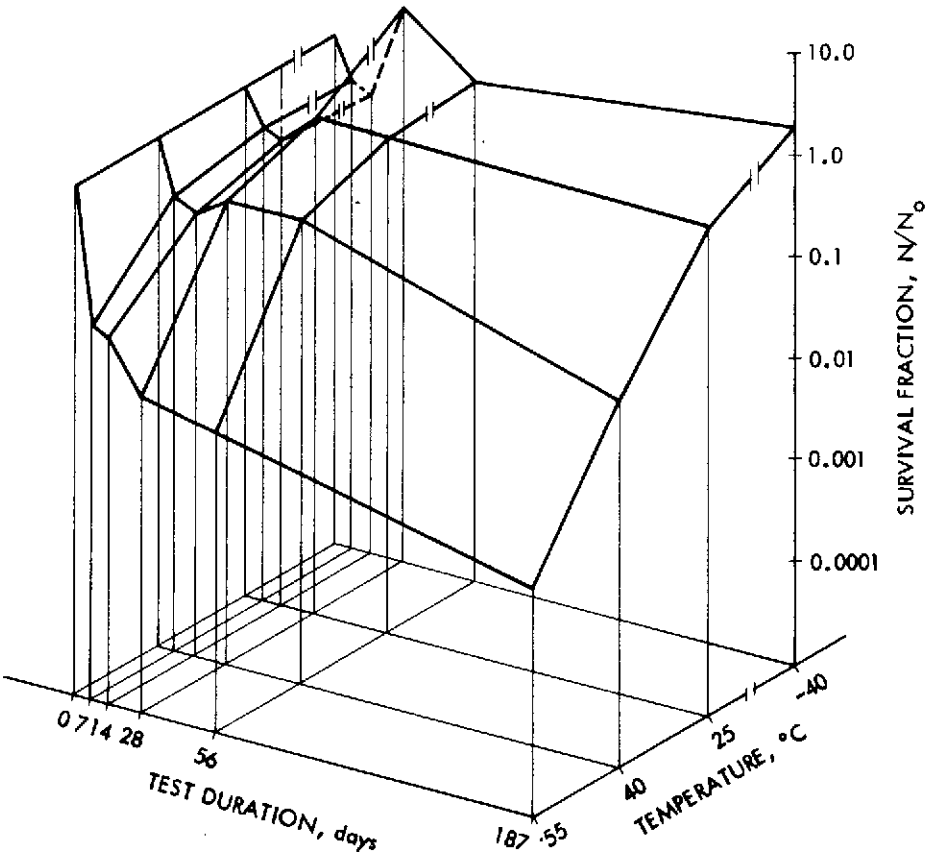

Fig. 2-C.6. Interaction of vacuum duration and temperature on combined spacecraft isolates (Spores)

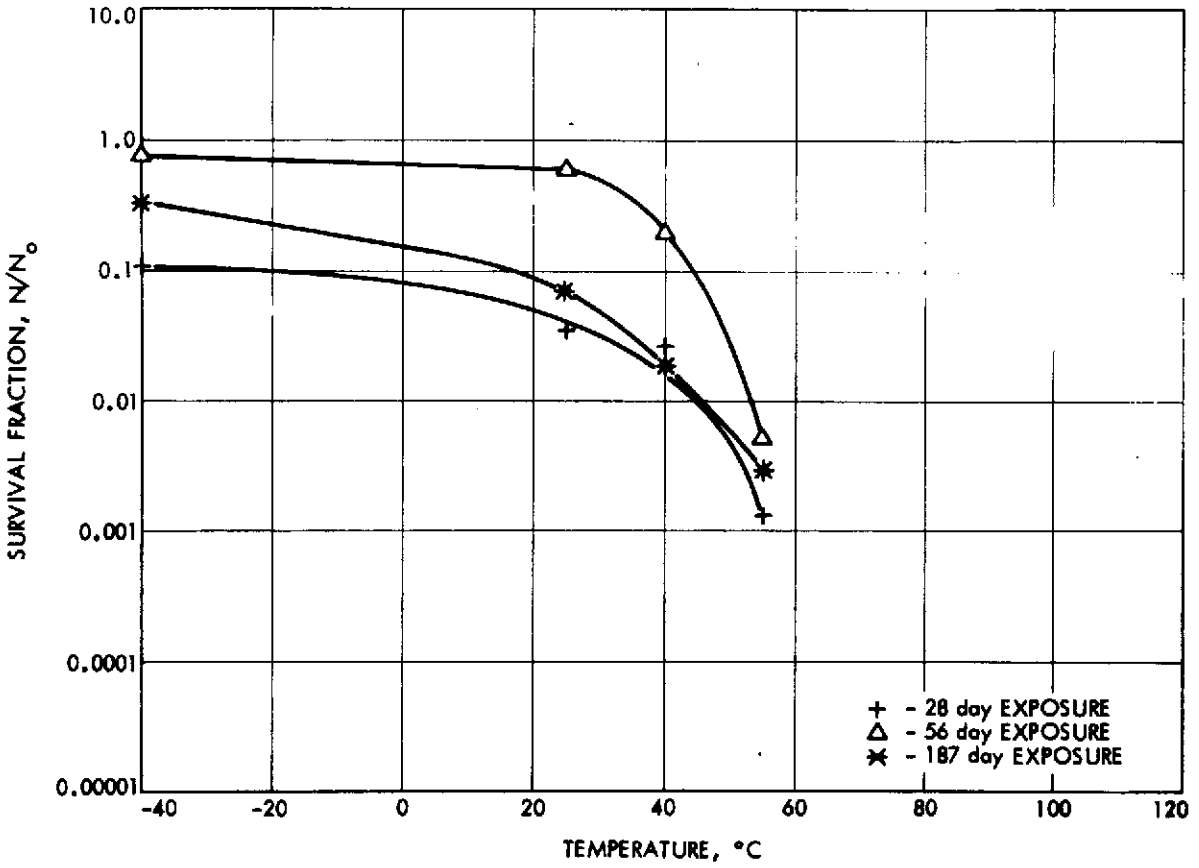

Fig. 2-C.7. Summary of vacuum-temperature studies (Vegetatives)

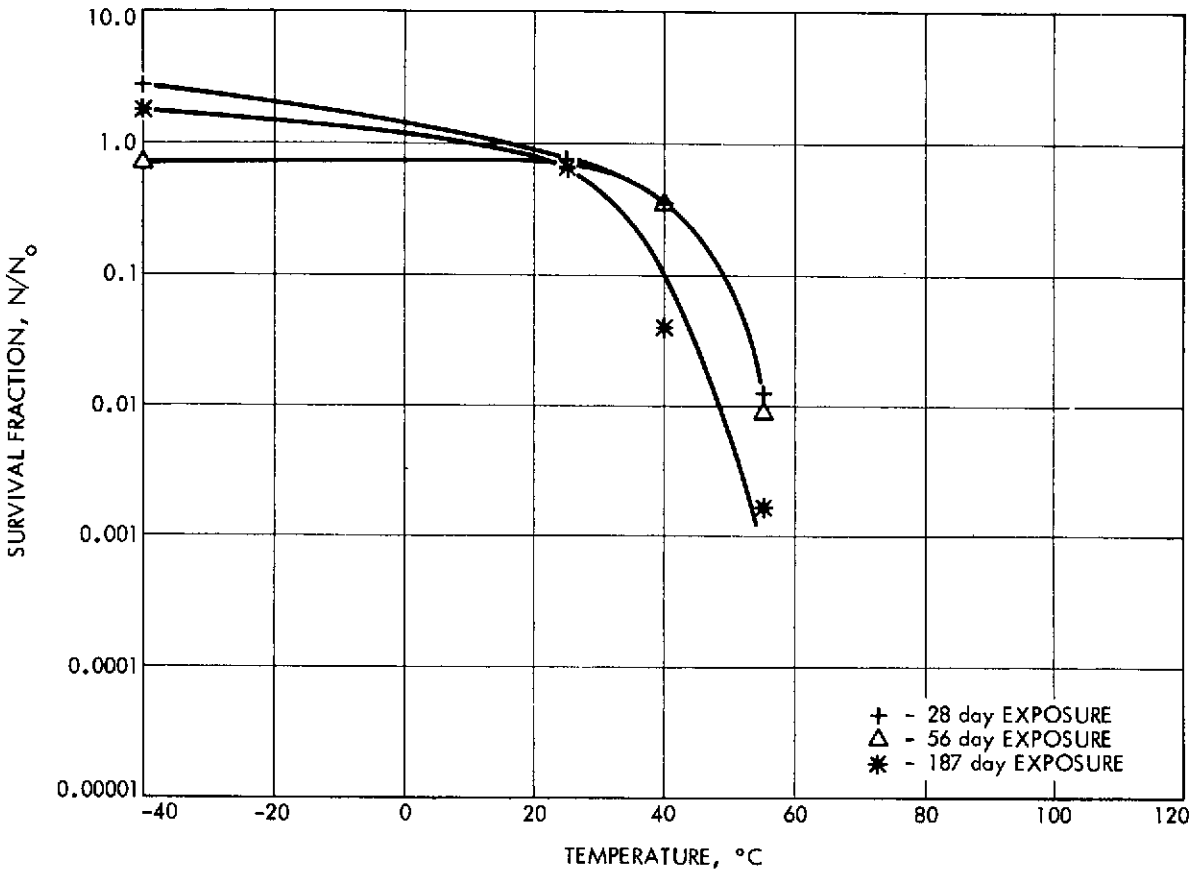

Fig. 2-C.8. Summary of vacuum-temperature studies (Spores)

SECTION III

POST LAUNCH RECONTAMINATION STUDIES
(NASA No. 193-58-62-03)

Contents

Subtask A
para. 3.1

Title and Related Personnel

POST LAUNCH RECONTAMINATION STUDIES

Cognizance: J. Barengoltz

Associate Personnel:
C. Bauerle (Bionetics)
R. Gildersleeve (Bionetics)
E. Robinson

3.1 POST LAUNCH RECONTAMINATION STUDIES

3.1.1 Subtask A Introduction

The objective of this task is the development of an analytical technique for the evaluation of the probability of the relocation of particles from nonsterile to sterile areas on a spacecraft. The recontamination process is important for all multiple missions with separate microbiological burden allocations for various major spacecraft systems, and critical for life detection experiments that risk contamination from nonsterile components.

The approach has been to study the effects of typical mission environments on the distribution of particles on spacecraft surfaces both analytically and experimentally.

The analysis consists of three logical components, which have been reflected in the effort: (1) particle adhesion, (2) dynamic release mechanisms, and (3) particle transport. The effort in particle adhesion has been principally a particle release experiment, together with analytical work and attempts to correlate other data found in the literature and elsewhere. Under dynamic release mechanisms, the modelling of meteroid impacts has continued. The other important release mechanism during the spaceflight phase, pyro firings, has been treated and reported earlier. The particle transport study is an analytical effort which includes the development of codes for spacecraft geometry and orientation, forces acting on released particles, and trajectory.

3.1.2 Significant Accomplishments

3.1.2.1 Particle Adhesion Force Study. The particle adhesion force study has been addressed to the experimental verification of a previously reported analytical model (Ref. 1). During the previous fiscal year a test facility was designed and fabricated. A schematic of this facility is shown in Fig. 3-A.1. The preliminary results obtained in that period and the description of the facility operation have been presented in Ref. 2. A test plan, also detailed in Ref. 2, designed to provide data to verify or to modify the analytical model, was inaugurated in the first half of the current fiscal year. As reported in Ref. 3, the tests with closely-sized glass beads in vacuo have been completed.

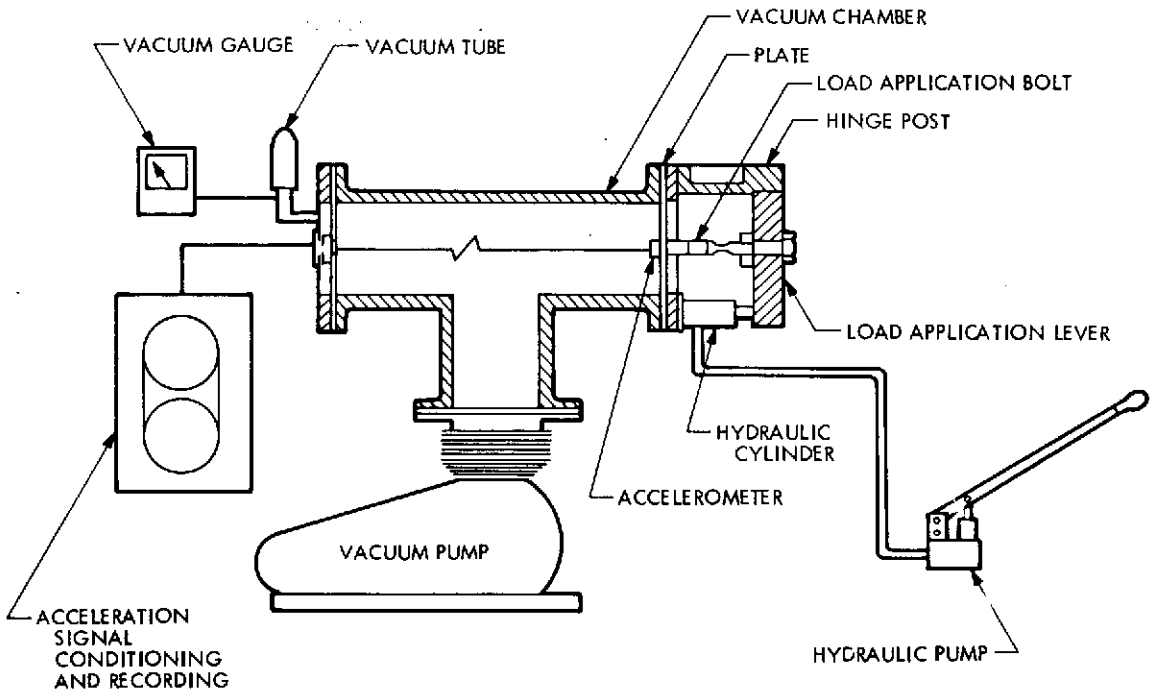

Fig. 3-A.1. Particle adhesion experimental apparatus

During this reporting period the data has been analyzed and several conclusions drawn. For a given particle size, retention was occasionally observed at an acceleration level greater than that where all the glass beads were removed on other runs. This anomalous retention is attributed to variability in surface conditions, although a standard cleaning procedure was employed. Due to this effect, the most one could extract from the data was a conservative threshold acceleration for each particle size. An important dependence on the relative humidity during the seeding operation was also observed. Finally, the threshold was found to vary inversely as the particle diameter. This finding implies an adhesion force proportional to the particle surface area.

A new empirical model which takes into account the conclusions above has been devised:

$$a_t = \frac{K}{D}(1 + RH) \tag{1}$$

where a_t is the threshold acceleration for removal of particles of diameter D, seeded at a relative humidity RH (%), and K is an empirical constant.

This model represents an extensive revision of the previous model (Ref. 1). The previous model predicts two parameters, a characteristic acceleration a_o and a characteristic transition parameter t. The latter parmeter describes the sharpness of the transition from complete retention of particles at low levels of acceleration to complete release at high levels. As stated, the data cannot provide a value for this parameter. The prediction for the characteristic acceleration a_o in units of kilo-gee (kG) is:

$$a_o = \frac{2 \times 10^{-4}\,(0.4 + 0.006\ RH)}{\pi\, D^2\, \rho\, g} \tag{2}$$

where ρ is the particle density (g μm^{-3}), D is the particle diameter (μm), g is the acceleration due to gravity (980 cm sec^{-2}), and RH is the relative humidity (percent) during release. Note that the new model, Equation 1, has the acceleration inversely proportional to the particle diameter. This dependence provided a far superior fit to the data than one can be obtained with the old model, Equation 2. Also the relative humidity parameter in the old model is identically zero in vacuo, but the new model allows a dependence on the relative humidity during seeding, which is not zero. The results of the data analysis and the empirical fit are summarized in Table 3-A. 1. The empirical constant K has been determined by the D = 44 μm data.

In an attempt to obtain improved particle adhesion data, a feasibility study on the applicability of acoustic emission detection technology was conducted. Acoustic emission detection exploits the fact that highly localized transient phenomena in materials radiate stress waves. These low intensity waves may be detected with piezo-electric transducers and large amplification factors.

Table 3-A.1. Particle Adhesion Test Results

Particle Diameter, μm	Relative Humidity, %	Threshold Acceleration, kG	
		Exp.	Model
20	48	8.0	5.0
44	48	2.9	2.9
63	23	0.8	1.0
88	30	0.6	0.9
105	40	1.0	1.0

Electronic signal processing and interpretation yield information on the time of the event and its size. In principle, the impacts of the small particles released from a surface as the result of a simulated meteoroid impact should be detectable by this technique.

The advantages offered by this new approach are:

1) Capability with realistic samples where optical counting is difficult

2) A direct measurement of ejection velocity

3) A direct experimental verification with glass beads of the combined particle adhesion and meteoroid impact models

4) A direct experimental link from meteoroid impact parameters to released grains for real spacecraft materials and contaminants.

All of these capabilities arise from the real time nature of these measurements, in contrast to before and after optical data. Item 3), for example, has been attempted elsewhere, but an actual optical count of the glass beads released is not feasible. Items 1) and 4) take advantage of the indifference of acoustic emission detection to the optical properties of the particle to be detected. As will be shown in para. 3.1.2.2, analysis has shown that the ejection velocity 2) is an important parameter.

At this time all of the preliminary experiments have been successful (Ref. 4). The results of the feasibility study indicate that particles of the mass and velocity of interest may be detected. Signal processing to directly display the number of impacts at low repetition rates and to infer the number of particles (of known mass) in a cluster has been demonstrated. The measurement of a crude velocity by clocking the interval from initial release to particle impact on the detection plate has been accomplished. Other experiments have provided information on accuracy and sensitivity.

3.1.2.2 Meteoroid Impact Study. The meteoroid impact study consists of a series of analyses for different conditions and geometry to provide the acceleration of struck surfaces and an experimental verification task. The code development of the analyses due to Yang (Ref. 2) is still in progress and almost complete. These new solutions for a thin plate and a semi-infinite solid call for a Fourier transform treatment which proves to be unfeasible computationally. JPL programming consultants have developed an alternate approach. The code development for Yang's punctured plate analysis has been stopped because an adequate alternative treatment is available. Because of the delays in obtaining operational codes, simple classical analyses have been performed, and the computer codes are complete. These codes treat the thin plate and the semi-infinite solid cases.

A preliminary approach to the problem of relating the loading function input of all the meteoroid analyses to the meteoroid impact parameters: mass, size, and velocity has been developed. Work is continuing in this area to refine the approach. The computer programs have been exercised; however, some results are presented in Figs. 3-A.2 and 3-A.3. In both figures the maximum surface acceleration response due to the loading function corresponding to a specified meteoroid impact is shown plotted against the distance from the center of impact. The struck surface is 0.125 inch aluminum plate.

Figure 3-A.2 is the result for a moderate impact, with an 0.8 Joule kinetic energy and other parameters as shown. For impacts of this size and smaller, the surface acceleration is significant (i.e., in the kilo-gee range) only within distances of a few plate thicknesses. On analytical grounds, the

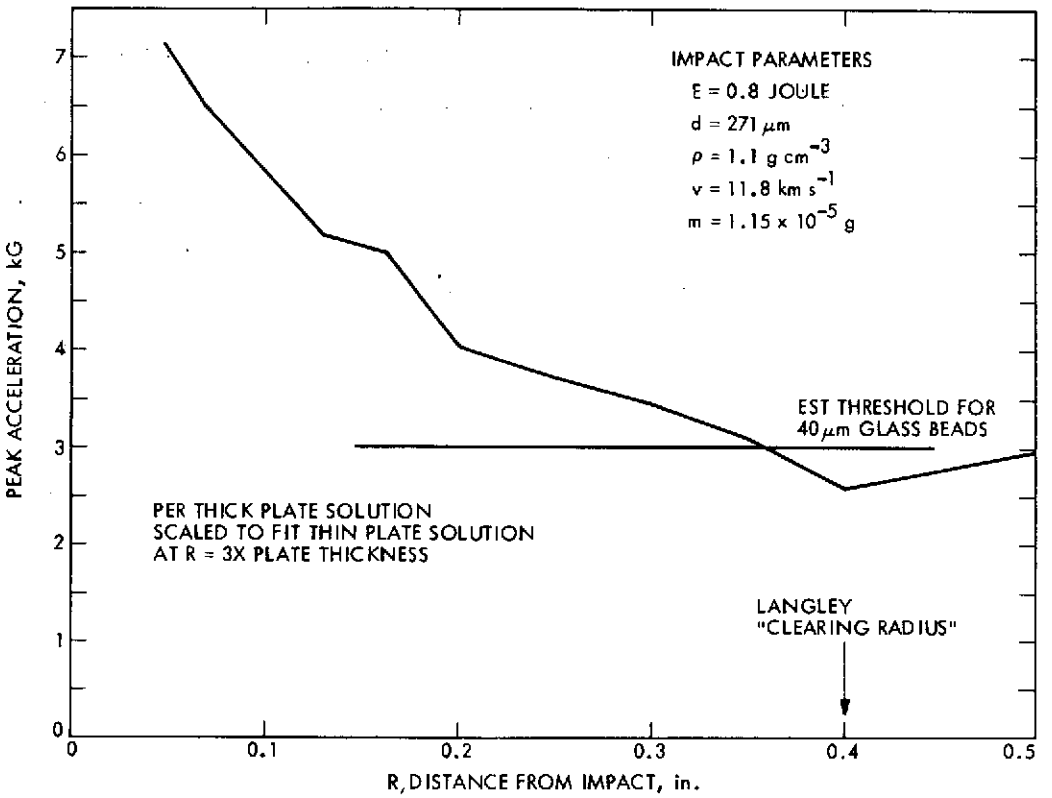

Fig. 3-A.2. Meteoroid impact analysis results (case I)

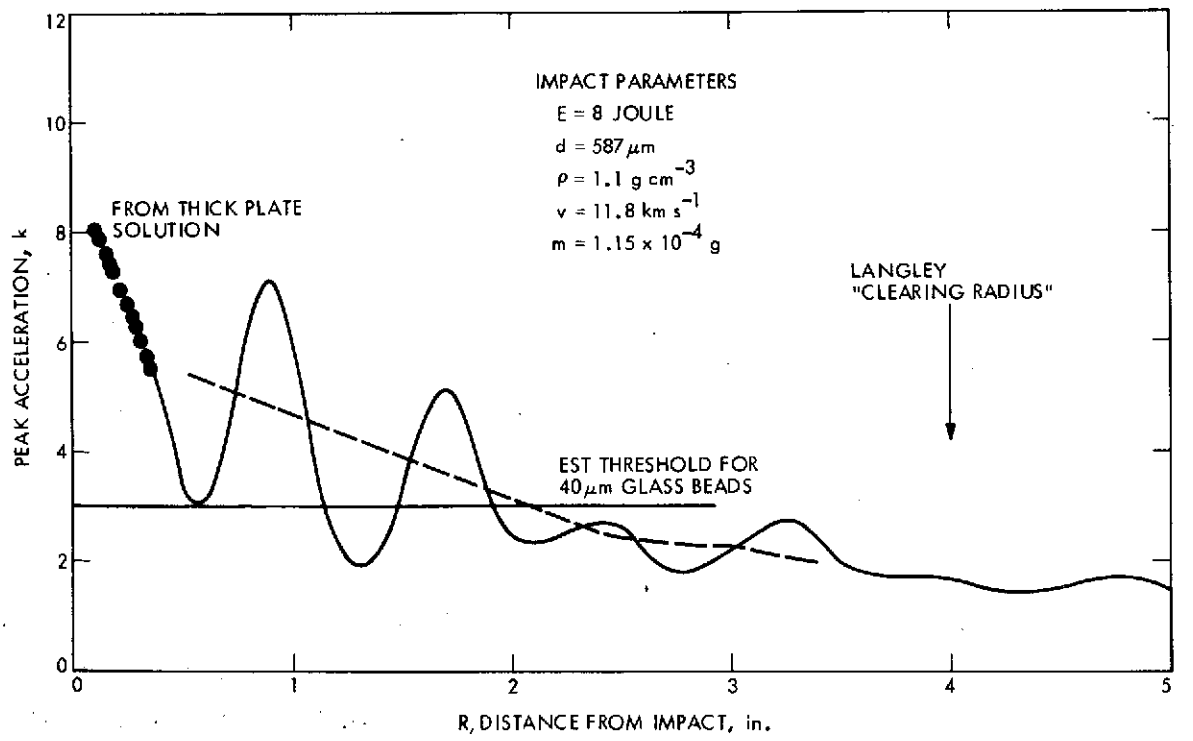

Fig. 3-A.3. Meteoroid impact analysis results (case II)

response for such distances is better described by the semi-infinite solid analysis. However, this program may produce an unnormalized result because a real plate has a finite thickness. Thus the semi-infinite or thick plate solution has been normalized to match the thin plate solution at a distance of three plate thicknesses.

The case of a larger impact, 8 Joule kinetic energy, is shown in Fig. 3-A.3. For this case, the surface acceleration persists at significant levels at much greater distances from impact. As in the other case, the renormalized contribution from the semi-infinite solid solution is indicated for small distances from the impact. The dashed line serves to indicate that the oscillations in the plot are mostly artificial and due to approximations in the analytical solution. Real materials are expected to produce a more damped acceleration profile.

Finally, a 3 kilo-gee estimate for the threshold acceleration for the removal of 40 μm glass beads is indicated on both Fig. 3-A.2 and 3-A.3. This value has been extracted from the particle release analysis described in the previous para. 3.1.2.1. The intersection of this estimate with the acceleration response curve provides a gauge of the extent of the surface from which the particles would be removed. This clearing radius, as the concept is commonly known, is a most important parameter. The particular values of the meteoroid parameters chosen were selected to match the values obtained experimentally by a research group at Langley Research Center (LRC) (Ref. 5). LRC results for the clearing radius with 40 μm glass beads are also shown. Although the agreement between these experimental values and the results of this analysis is fair, several problems render the comparison quite preliminary. Many of the meteoroid parameters in the LRC experiment were not measured. The cleanliness of the plates has been shown by the LRC group to be a critical variable. Thus, the removal acceleration found in JPL tests may not be relevant to LRC tests. Lastly, JPL analysis hinges on the relationship between impact parameters and the loading function, where work is still in progress.

3.1.2.2 Particle Transport Analysis. During this reporting period of 1 Jan through 30 June 1973, the analysis of the forces acting on released particles has progressed. Work has been centralized on the electrostatic

force, where the electric field due to the spacecraft-plasma system and the electric charge on the particle (grain) are required. In parallel, the spacecraft geometry and orientation and the particle transport codes have been integrated to an operational subprogram with dummy forces. Finally, this subprogram has been exercised in some simple two-dimensional geometries with the use of the one-dimensional electric field and the particle charging routines that have been developed. Some insight into the sensitivity of the recontamination process to physical parameters has been obtained.

The three-dimensional potential solution for an object moving relative to a plasma is very difficult even in the simplest geometry, a uniform conducting sphere. This situation, which has been solved implicitly by others, requires that the relative directed velocities (as opposed to the thermal, random velocities) of all components of the plasma be equal. These conditions are satisfied when all of the relative directed velocity is due to the object's motion. In the case of interplanetary spaceflight in the solar wind plasma, however, the proton component has a directed velocity which dominates its relative velocity, while the electron component by comparison is essentially at rest. Finally, the photoelectric effect produces yet another plasma component exactly at rest with respect to the spacecraft. Thus the potential problem is a much more difficult one than a mere complicated geometry to be approximated by known solutions for simple geometries.

The solution to the one-dimensional problem of a plate exposed to solar illumination, electrons, and protons has been found in the literature (Ref. 6 and 7). In this solution the positional dependence of the electric potential in equilibrium was expressed implicity in terms of the surface potential and the plasma parameters. An approximate explicit form for the potential based on this work has been developed which provides an approximate formula for the electric field as well. This analysis has been adapted into a computer code and the results have been published (Ref. 8).

In order to obtain numerical values for the potential and the field, the plasma parameters and the equilibrium surface potential are required. The pertinent parameters of the solar wind plasma are available (Ref. 9). For the photoelectron plasma, the typical experimental values obtained for ultra-clean

surfaces are expected to differ drastically from values corresponding to realistic spacecraft surfaces. However, a detailed experiment for realistic surfaces of several spacecraft materials has been reported by others. Finally, the equilibrium surface potential for these materials has been determined with the use of the parameters above and the requirement that the net current becomes zero at equilibrium.

Following the authors of Ref. 6 and 7, two classes of solutions to the problem were found, noted as monotonic and non-monotonic. However, the quantity of interest here, the electric field in the vicinity of the plate, is virtually the same for the two solutions. Some results for aluminum and silica are shown in Fig. 3-A.4. The most striking feature of these results is a fall-off of the field with distance at a far faster rate than the field for the case with

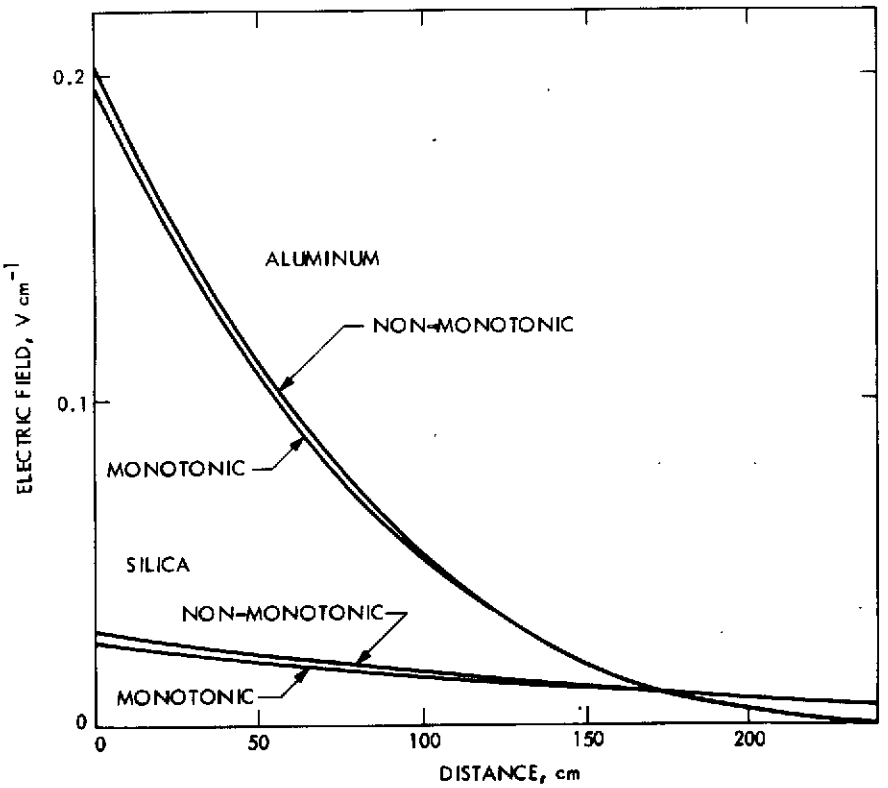

Fig. 3-A.4. One dimensional electric field

no photo-electric effect. The latter problem has an exact solution, a decreasing exponential, with an e-folding distance equal to the Debye length. For the solar wind plasma parameters, the Debye length is about 1200 cm. In contrast, the e-folding distance, as determined by an exponential fit to the results given in Fig. 3-A.4, is about 80 cm for aluminum and 200 cm for silica in our analysis. Thus the effect of the photoelectrons is to dramatically reduce the effective range of the electric field and to render the effective range of the electric field material dependent.

The solution to the problem of particle or grain charging requires many of the same considerations as the electric field problem. However, in this case only the surface potential is of interest and the time dependent solution for this quantity is needed. The surface potential may be related to the total charge on the particle for a simple geometry (i.e., a sphere). Since the particle is small compared to the relevant size parameters of the electric field, it may be treated as a point charge in calculating the force acting on it. However, because the particle is small, it will not equilibrate in a time that is short compared to the period of its movement when released. Thus the need for the time dependence arises.

Given the geometry of a particle and the potential-dependent currents flowing into it, one may express the charging rate in an implicit form. For the illuminated particle, these currents are a collimated proton current, an isotropic electron current, and the photoelectric current due to a collimated solar spectrum. For a spherical particle:

$$\frac{d\phi}{dt} = \frac{2.9 \times 10^{-9}}{R^2} \pi d \left[A_p + A_e + A_\nu \right] \tag{3}$$

$$A_p = \frac{n_p v_o}{4}$$

$$A_e = -\frac{n_e v}{4} \times \begin{cases} \exp\left(e\phi/kT_e\right) & \phi \leq 0 \\ \left[1 + 2e\phi/kT_e\right]^{1/2} & \phi > 0 \end{cases}$$

A_ν = photoelectron flux, dependent on ϕ

In this equation, the proton flux A_p depends on the number density n_p (m^{-3}) and the directed velocity v_o (ms^{-1}) and the electron flux A_e depends on the number density n_e (m^{-3}), the mean thermal speed $\bar{v}$(ms^{-1}) and the temperature kT_e (eV). The photoelectron flux A_ν is calculated numerically from the photoelectric yield data (Ref. 10), for the solar spectrum, material of the surface, and current surface potential. With A_p, A_e, and A_ν in units of $m^{-2}s^{-1}$, the particle diameter d in m and the heliocentric distance R in AU, one obtains $d\phi/dt$ in Vs^{-1}. Results of this calculation are shown in Fig. 3-A.5 for aluminum, silica, and graphite. The equilibrium surface potential may be inferred by the requirement that $d\phi/dt$ is zero at equilibrium. These values are also given in Fig. 3-A.5.

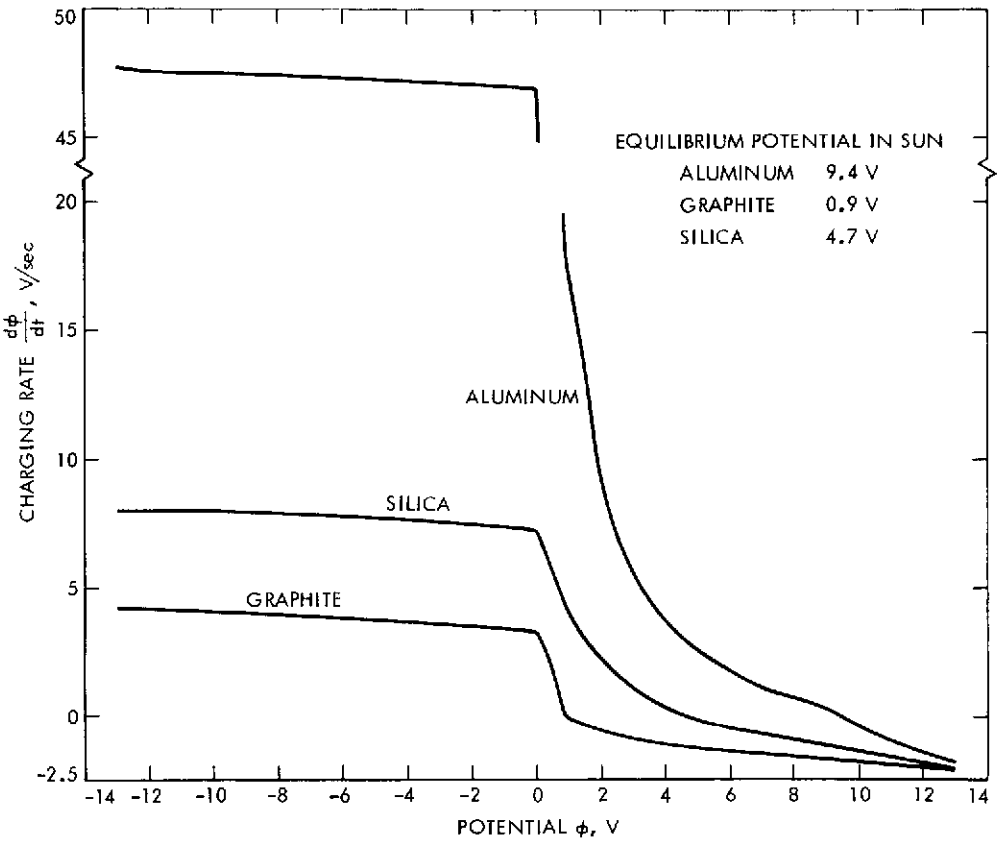

Fig. 3-A.5. Grain charging in sunlight

The particle in the shade (of the spacecraft) may be calculated in an analogous manner. Here, to a first approximation, $A_p = A_\nu = 0$ and A_e is unchanged from Equation 3. However, the resulting expression for $d\phi/dt$ would not equilibrate. The particle would continue to charge more negatively forever, with $d\phi/dt$ tending to zero as ϕ tended to $-\infty$. In reality, other effects, such as thermionic emission, field emission, secondary emission and the accretion of protons attracted into the shade, would act to limit the potential at approximately $-3\ kT_e/e$. The effort is continuing in this area, but at present the consideration of a reasonable model for A_p in the shade appears to provide the necessary balance.

With the addition of the solar radiation pressure to the electrostatic force based on the preceding discussion, the trajectory of a grain in some simple but important geometries may be calculated. The results for the two simplest cases considered are shown in Fig. 3-A.6. In the one-dimensional

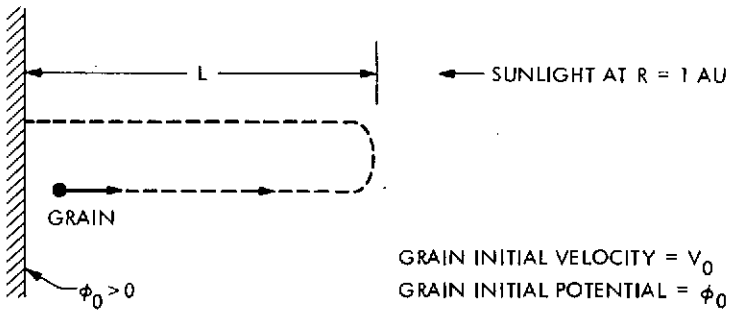

	D PARTICLE DIAMETER, μm	V_0 NORMAL VELOCITY, m/sec	L TURNAROUND, m
CASE I SUNLIGHT $\phi_0 = 12$ V	10 - 100	0	∞
CASE II NO SUNLIGHT $\phi_0 = 6$ V	20	0.08	∞
	20	0.05	3.6
	20	0.02	1.0
	80	0.02	6.0
	100	0.02	∞
	20	0.01	0.4
	100	0.01	1.7

Fig. 3-A.6. Particle trajectory calculations

problem of an aluminum plate with a +12 V surface potential under normal illumination, a particle is displaced from the surface with a normal velocity v_o and an initial potential ϕ_o, equal to +12 V. Although the electrostatic force acts always to repel the particle from the plate, the solar radiation force acting on it tends to push it back toward the plate. At some distance from the plate, the electrostatic force will have decreased due to the reduction of the field (see Fig. 3-A.4) so that it just balances the solar radiation force, which is proportional to D^2, where D is the particle diameter. However, the most interesting parameter, the turnaround distance where the velocity is zero, will occur at an even greater distance. The turnaround distance will be significantly larger than 4 m for all values of diameter considered, even with v_o equal to zero. In terms of the two-dimensional problem, a released particle will migrate parallel to the surface with a constant speed given by its original component parallel to the surface, while it also moves normally to the surface as discussed above. A consideration of the period of the trajectory shows that the lateral displacement would be very large even for a very modest parallel velocity component. Thus the particle cannot, in the practical sense, return to the spacecraft.

In the second case shown in Fig. 3-A.6, the particle and the aluminum plate are in the shade, but the plate has a positive potential of 6 V. This situation would occur if the plate were connected electrically to another metal surface which was itself illuminated. In this case the displaced particle is initially repelled by the electrostatic force but eventually discharges. At the point where the particle has assumed a negative potential, it is attracted back toward the plate. However, the electric field decreases farther from the plate, and the attractive force may be very small. As in the previous case, therefore, a finite theoretical turnaround distance still may be defined, beyond the point where the particle obtains zero net charge. Examples where turnaround occurs beyond 10 m are labeled as ∞.

The most important result of these considerations is the emergence of the particle ejection velocity as a critical parameter. Note, for example, that a 20 μm particle will escape if its ejection velocity exceeds 0.08 m s^{-1}, but will return for v_o = 0.05 ms^{-1} and will return sooner for v_o = 0.02 ms^{-1}.

This effect also depends on particle size. A larger particle has a smaller escape velocity. Thus a 100 μm particle will escape at $v_o = 0.02$ ms^{-1} but not at $v_o = 0.01$ ms^{-1}. All of the values presented in Fig. 3-A.6 are based on glass spheres, with a density of 2400 kg m^{-3}.

3.1.3 Future Activities

Work remains to be accomplished in each of the major areas of this task. Under particle adhesion, the particle release apparatus is currently being modified to employ acoustic emission detectors. Plans are formulated to repeat some of the glass bead experiments to verify the accuracy of this approach and to obtain velocity measurements. Then experiments will be conducted with realistic samples (dust with a known size distribution). If resources permit and a hypervelocity gun is available, a complete experiment, as shown in the schematic Fig. 3-A.7, will be conducted. Such an experiment would provide a direct verification of the combination of the particle adhesion and meteoroid impact models, including the loading function. In terms of the task, a direct connection between meteoroid impact parameters and the number and velocity of particles released would be made.

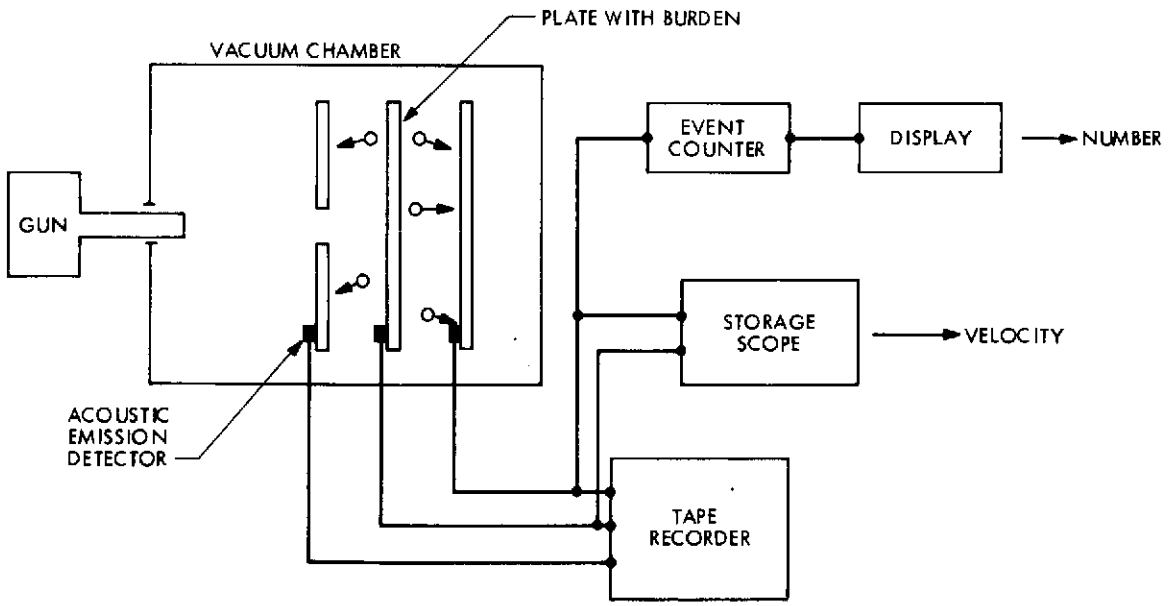

Fig. 3-A.7. Conceptual schematic for acoustic emission application to particle release

In the meteoroid impact analysis, the development of an appropriate loading function in terms of the meteoroid impact parameters will be completed. In addition, the computer coding of the new improved impact analyses will be accomplished. Analysis will be conducted to extract the relevant results in a more direct manner suitable for a complete program.

The development of a three-dimensional electric field is the goal in the particle transport analysis. This effort will involve calculations for the spacecraft wake region. In connection with this work, a charging model for the particle in the shade, in or out of the wake, will be fashioned.

Finally, a major effort in the integration of the various analyses and experimental results into a working program will be undertaken. A flow diagram indicating the logic of this program is shown in Fig. 3-A.8.

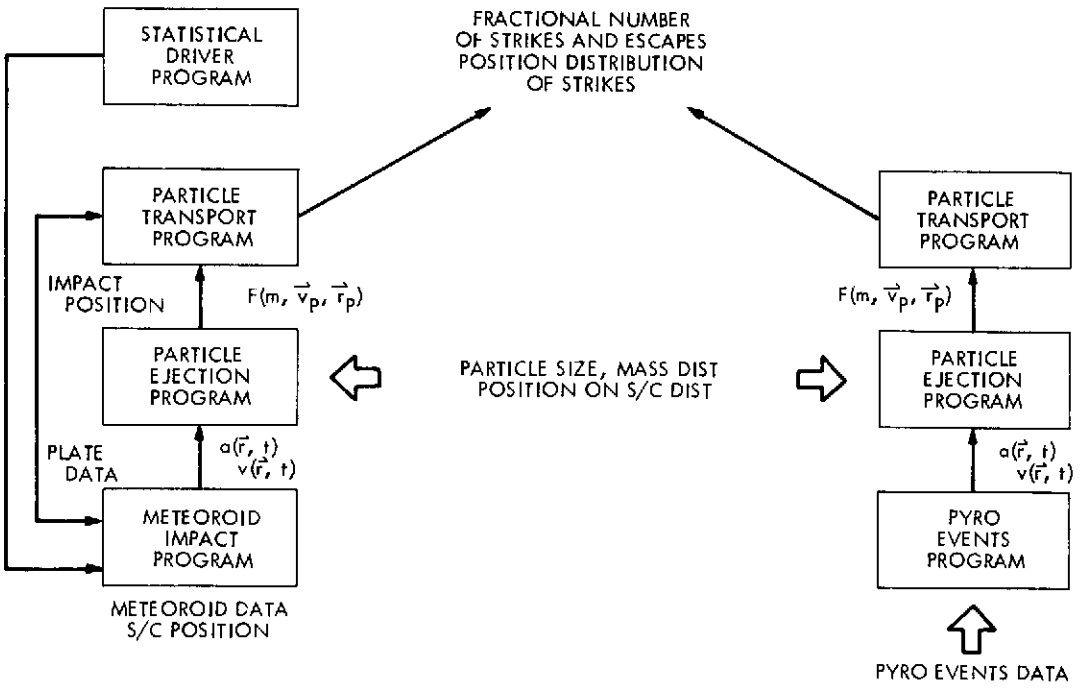

Fig. 3-A.8. Flow diagram for spacecraft recontamination analysis

3.1.4 Presentations

Barengoltz, J., "Post Launch Recontamination Studies," presented at NASA Spacecraft Sterilization Technology Seminar, Denver, Colorado, July, 1973.

3.1.5 Publications

Barengoltz, J. and Bauerle, C., "The Electric Field in the Vicinity of a Photo-Emitting Plate in a Plasma," JPL Quarterly Technical Review, Vol. 3, No. 1, p. 26, April, 1973.

3.1.6 References

1. Haudenschild, C., "Mathematical Model of Particle Adhesion Force to Surfaces," JPL IOM, 9 March 1971.
2. Planetary Quarantine Annual Review, Space Technology and Research, July 1971 - July 1972, JPL Document 900-597, February, 1973.
3. Planetary Quarantine Semi-Annual Review, Space Research and Technology, July 1972 - December 1972, JPL Document 900-608, 1973.
4. Robinson, E., "Application of Acoustic Emission to Microparticle Impact Methods," JPL IOM 13 June, 1973.
5. Humes, D. H., et al., private communication.
6. Fu, J. H. M., "Surface Potential of a Photo-Emitting Plate," J. Geophys. Res., Vol. 76, No. 10, 1971.
7. Guernsey, R. L., and Fu, J. H. M., "Potential Distribution Surrounding a Photo-Emitting Plate in a Dilute Plasma," J. Geophys. Res., Vol 75, No. 16, 1970.
8. Barengoltz, J., and Baurle, C., "The Electric Field in the Vicinity of a Photo-Emitting Plate in a Plasma," JPL Quarterly Technical Review, Vol. 3, No. 1, April, 1973.
9. Divine, N., "Summary of Solar Wind Properties," JPL IOM 2947-71-151, 21 December 1971.
10. Feuerbacher, B., and Fitton, B., "Experimental Investigation of Photoemission from Satellite Surface Materials," J. Appl. Phys., Vol. 43, 1972.

SECTION IV

SPACECRAFT CLEANING AND DECONTAMINATION TECHNIQUES
(NASA No. 193-58-63-02)

Contents	Title and Related Personnel
Subtask A para. 4-1	PHYSICAL REMOVAL OF SPACECRAFT MICROBIAL BURDEN Cognizance: H. W. Schneider Associate Personnel: E. Roos (Bionetics)
Subtask B para. 4-2	EVALUATION OF PLASMA CLEANING AND DECONTAMINATION TECHNIQUES Cognizance: D. M. Taylor Associate Personnel: R. L. Olson (Boeing) S. J. Fraizer (Boeing) R. B. Gillette (Boeing)

4.1 PHYSICAL REMOVAL OF SPACECRAFT MICROBIAL BURDEN

4.1.1 Subtask A Introduction

Present planetary quarantine constraints for flyby and orbiter vehicles require maintaining the microbial burden on the spacecraft below a certain critical level. State-of-the-art clean room facilities and contamination control techniques do not assure that this critical level can be maintained throughout necessary assembly and test operations.

Previous activities under this task concentrated on the study of vacuum cleaning techniques with and without the aid of a brush. These techniques are the primary methods applied in present spacecraft operations. A test device was developed that allowed for the simulation and evaluation of typical techniques and surface conditions under controllable and repeatable test conditions. As described in detail in JPL Document 900-597, the following major problems were identified:

1) Brushes efficiently detach particles of the smallest detectable size (2-3 μm) but entrainment into the flow is extremely poor. The flow resistance across the bristle is very high, and flow velocities near the surface are too low to accomplish entrainment and transport of the detached particles. Consequently, the bristles quickly become saturated with particles and the brush becomes a particle source rather than a cleaning tool. To avoid this, frequent cleaning, and/or perhaps, if use requires, biological decontamination of the brushes during or between uses is strongly recommended.

2) Vacuum flow alone (without the aid of a brush) efficiently detaches and removes particles larger than 10 μm size if 1) the surface is dry; 2) flow velocities are near critical (choked flow) and 3) nozzle stand-off distance from the surface is approximately 150-200 μm. The removal efficiency drops off sharply at larger stand-off distances. The cleaning of moist and fingerprinted surfaces is very inefficient under any of the conditions tested.

Since, at choked flow conditions, the removal capability of vacuum flow is exhausted, the only means to further increase the detachment force or to increase the usable standoff from the surface was to increase the flow density. To accomplish this the pressure of the expansion source had to be raised. The effort during the reporting period concentrated on the evaluation of blow-vacuum techniques where particle detachment is accomplished by means of jet expansion from a pressure source (at higher than atmospheric pressure). In this case the vacuum flow only has the function of removing detached particles from the area. The results obtained and the conclusions drawn from these latter studies are covered and discussed in this report.

4.1.2 Approach

The application of the jet-blow in addition to vacuum flow has introduced a large number of possible variables. These variables selected for evaluation included the blow-pressure, the blow angle, and typical working pattern such as spot-blow, sweeping with and against the flow, as well as repeated sweeping over the same area. The parameters of the vacuum flow were kept constant. It was assumed that an existing facility system would be used to provide a low pressure/large volume flow sufficient to accomplish the removal of the detached particulates.

4.1.2.1 Experimental Techniques. As in previous studies, 5 cm × 5 cm (2 × 2) optical glass slides were used seeded with test particles. The slides were cleaned prior to seeding with freon TF followed by a wipe with isopropyl alcohol. Typical abnormal surface conditions, such as oiliness and moisture, were simulated by fingerprinting the samples prior to seeding, and by placing a seeded sample into a refrigerator for 15 minutes. The latter technique would induce a temporary fogging when the slides were returned to the room environment (25-28° C, 45 percent - 55 percent RH).

Glass beads were chosen as the primary test material for evaluating and comparing the effectiveness of different techniques. Two size groups were tested which ranged between 0-5 and 5-10 μm. Figure 4-A.1 shows the size distributions found on seeded samples prior to testing. The beads were dried and shaken prior to testing using the earlier described dip-and-tap method for

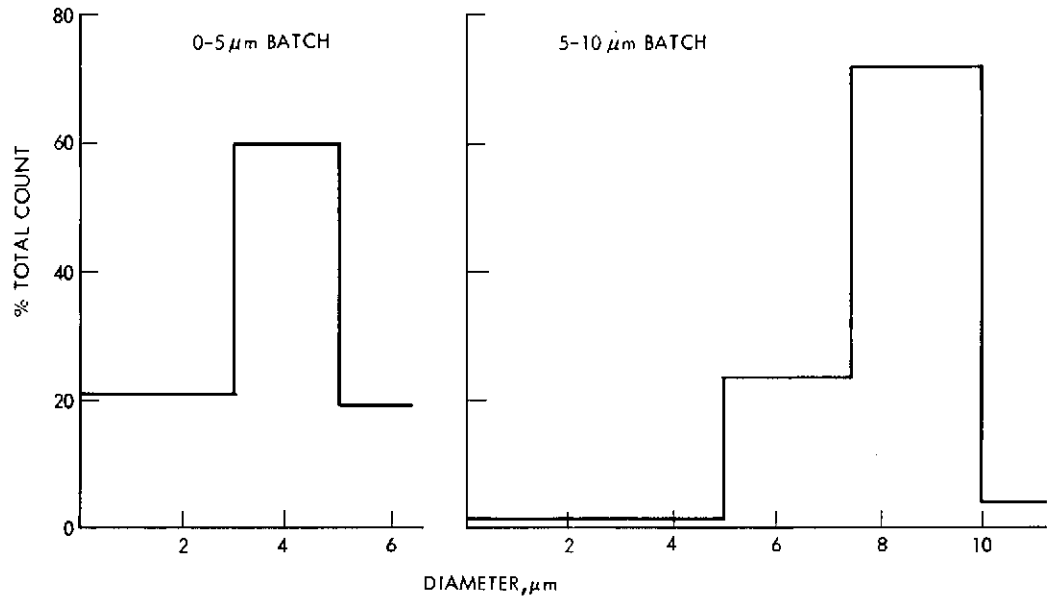

Fig. 4-A.1. Typical size distribution of glass beads used for test

seeding until an initial concentration of approximately 1000 particles per mm^2 was obtained. Counts of all particles ≥ 3 μm were taken from a 0.25 mm^2 area in the center of the sample prior to and after each test.

It is well known from literature and from previous tests that the surface adhesion characteristics of glass beads are different from those of dust. A small number of selected tests were conducted with dust for comparison before drawing final conclusions. In this case the samples were seeded by placing them for a number of days in an undisturbed office area until a concentration on the order of 10-15 particles per mm^2 was collected. Counts and size determinations were made from a 5 x 1 mm^2 area in the center of the samples prior to and after each test with dust by measuring the largest dimension (Peret's diameter) normal to the flow. Typical surface conditions were simulated as described above for glass beads.

4.1.2.2 Test Apparatus. The test apparatus is shown in Fig. 4-A.2. It is the same device used in previous studies but modified to accommodate a blow nozzle. Figure 4-A.3 shows the schematic of the device seen in the photo, Fig. 4-A.2. On top is the 100X microscope (1); the sample slide (2) is placed

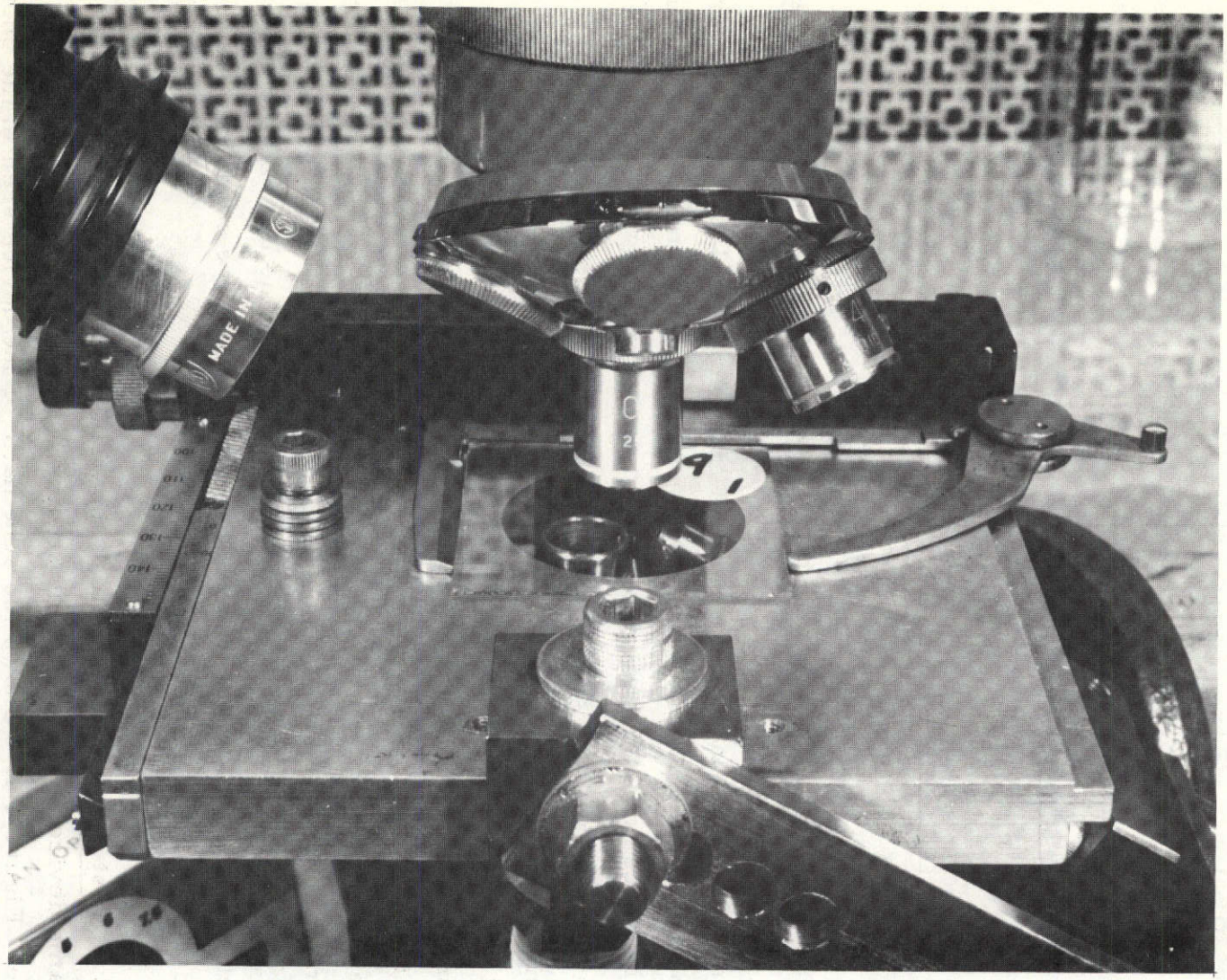

Fig. 4-A.2. Test apparatus (as seen in schematic, Fig. 4-A.3)

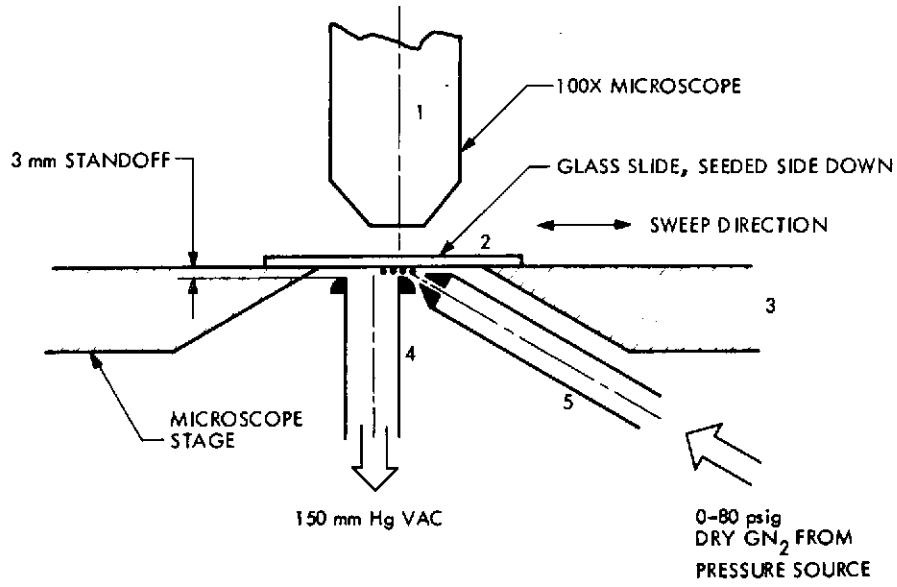

Fig. 4-A.3. Apparatus schematic

on the microscope stage (3) with seeded side down, and underneath the vacuum nozzle (4), and the blow-nozzle (5).

The vacuum nozzle has a rounded lip and was adjusted for a constant 3 mm standoff from the sample surface throughout all tests. The inner diameter had to be increased from 6.5 mm to 13 mm (compared to the old apparatus), to comply with the larger (3mm) standoff. The facility vacuum system provided for an average vacuum of 150 mm Hg under these conditions. The blow nozzle was aimed at a point on the sample surface where vacuum flow velocities should be a maximum. The nozzle could be pivoted about this point between 30 and 57 degrees from the sample plane without changing the slant range of the free jet, which was adjusted for 5 mm during all tests. The flow controlling section of the blow nozzle consisted of a 1.6 mm diameter, cylindrical orifice representing approximately 2 percent of the vacuum nozzle from a pressure source through a needle valve. Pressures up to 80 psig across the nozzle orifice could be produced with the existing set-up.

4.1.3 Significant Accomplishments

4.1.3.1 Tests with Glass Beads.

1. Blow Angle. The choice of the blow angle was one of the first problems to be resolved. Because of the low adhesion of the glass beads to dry surfaces, fogged samples were chosen to make the tests conservative. The results are plotted in Fig. 4-A.4. Each data point represents the efficiency obtained with a 5 second spot-blow at the indicated pressure.

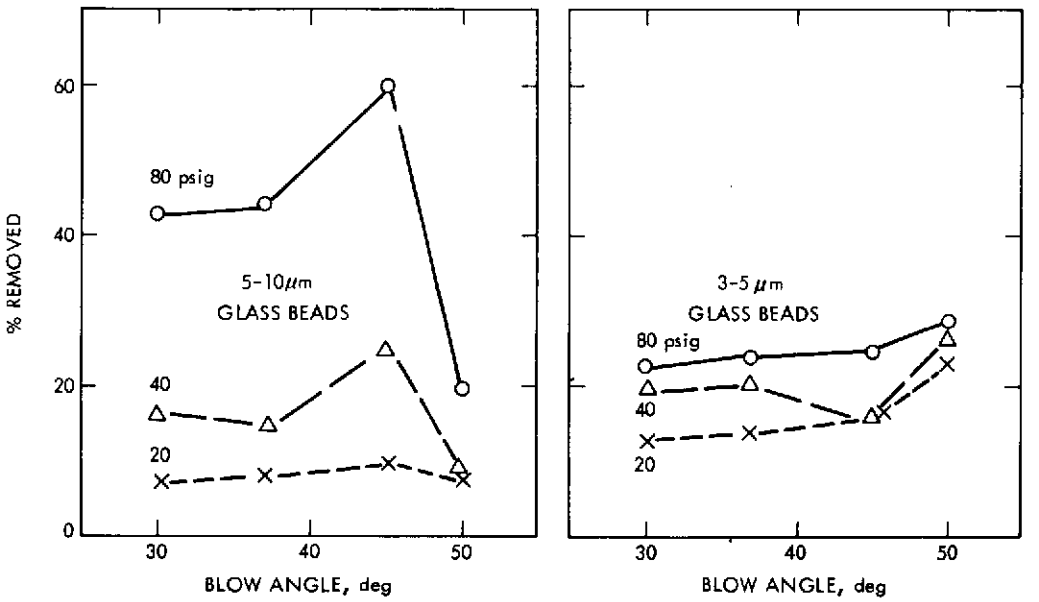

Fig. 4-A.4. Removal efficiency vs blow angle and pressure

For the 5-10 μm size group a strong effect of the angle on the removal efficiency, that becomes increasingly pronounced with pressure, is evident. This can be explained with the known relations between the jet momentum and the compression shocks formed upon deflection from the surface. An analytical treatment of the 3-dimensional flow (fan-pattern) forming upon impact of the jet on the surface was considered beyond the scope of the present effort.

For the 3-5 μm size group the blow angle does not show any significant effect. This is, probably because the conditions in the sublayer are not

effected by the aerodynamics of the main jet. Since the removal of particles ≧ 5 microns was of primary interest, it was concluded that all follow-on tests should be conducted at a 45 degree angle. As described in para. 4.1.3.1, sub-para. 5, this also appeared to be the best choice from the reentrainment standpoint.

2. Blow Pressure. The blow pressure required for efficient removal is an important parameter when considering surface compatibility. The results are plotted in Fig. 4-A.5. Each data point represents the

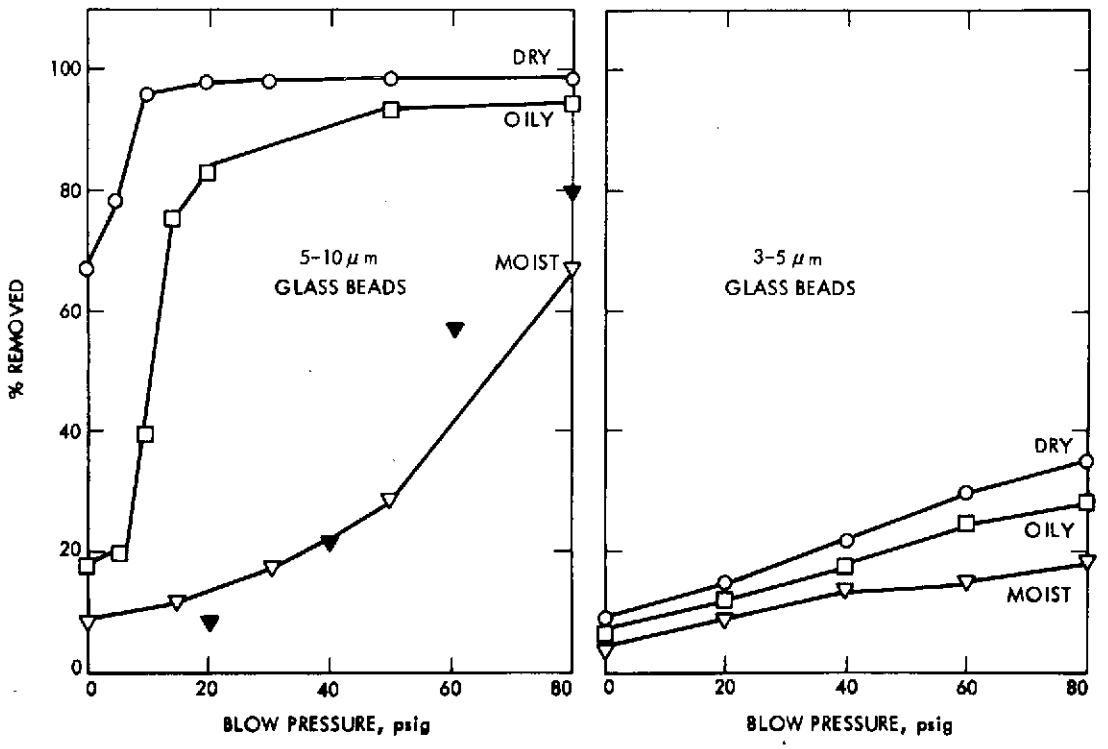

Fig. 4-A.5. Removal efficiency vs blow-pressure for different surface conditions (45 deg blow angle)

efficiency achieved with a five second spot blow at the reference area in the center of the sample. Two determinations were made for each of the surface conditions and size ranges indicated. The data points at zero pressure represent the efficiencies achieved with the vacuum flow alone. Two different techniques were applied. (a) The same sample was used to establish the data

points, indicated by the curves connecting the open symbols (o, Δ, □) with each other. (b) A completely new sample was used for each data point (blowing each sample only one time). These data are represented by the solid symbols. This latter method was mainly applied for a comparison of time effects and a possible deterioration of the removal capability at higher pressures.

For the 5-10 μm size group a considerable improvement of the removal capability over vacuum flow alone is evident, particularly if the surface is wet or oily. On the dry surface almost all of the particulates were removed at the critical expansion pressure (15 psig). For the blow-cleaning of oily surfaces, pressures of approximately 50 psig would have to be applied to achieve maximum efficiency. Smaller pressures on the order of 15 psig, however, would already affect a strong increase of the efficiency, if compared to vacuum flow alone. The removal capability improves drastically with blow pressure on a moist surface, but the pressures required are high (> 80 psig).

For 3-5 μm glass beads, the blowing at the surface does not seem to efficiently remove particles under any of the conditions tested.

3. Sweep Pattern. Under practical conditions a relative motion between the cleaning apparatus and the sample will be involved. Fig. 4-A.6 shows the results of a series of tests where typical motions were simulated as they are likely to occur during actual cleaning operations. A separate sample was used for each test. Two determinations were made per data point. A fogged surface was chosen to make the test conservative, because glass beads on such a surface are more difficult to remove than on dry or oily surfaces.

The criterion for evaluation, plotted as the ordinate, represents the efficiency gained by use of the sweeping pattern related to the efficiency achieved with vacuum flow alone. The high gain factors achieved, in some cases, result from the small efficiency achieved with vacuum alone (see Fig. 4-A.5). Each size group shown represents a typical motion applied, such as a five second spot blow, a 1 cm sweep against, and with the flow; and a 1 cm double sweep starting against and with the flow as indicated by arrows on

Fig. 4-A.6. The sweeping motion was manually controlled, advancing at a rate of approximately 0.5 cm per second in either direction. The bars within each group represent the blow pressures applied.

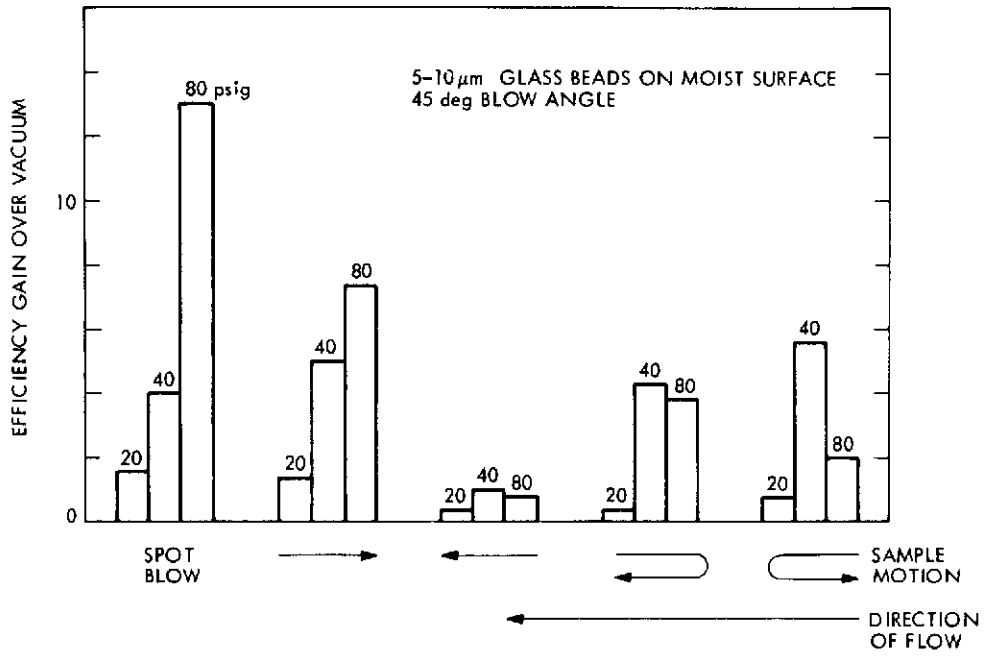

Fig. 4-A.6. Efficiency gain vs sweep pattern

At the high pressures (80 psig) the spot blow is most efficient, because the time exposure of the reference area is reduced by a factor of ten or more. For the two lower pressures tested (20 and 40 psig) time exposure does not seem to be a factor, but the direction of the sweep has a strong influence for all pressures tested. It is quite obvious that sweeping against flow is best. Except for the high pressure, a double stroke that ends with an upstream stroke is better than one that ends with a downstream motion. As could be observed under the microscope, recontaminating effects (particle migration without detachment) during the downstream motion are responsible for this.

In conclusion: (a) sweeping against the flow should be the preferred method, (b) single or multiple double-strokes should start and always end with an upstream sweep.

4. Repeated Cleaning. Another consideration is the gain to be expected by repeated sweeping over the same area. To establish this, tests were conducted on six separate samples seeded with 3-5 and 5-10 μm glass beads, using double strokes ending upstream. A moist surface was chosen for more indicative results. Counts were taken prior to and after each test.

The results are plotted in Fig. 4-A.7. The criterion for evaluation here is the efficiency gain over that achieved during the first stroke. A strong improvement that becomes increasingly pronounced with pressure is evident. It appears, however, that the gradient tends to level off after a few strokes. At the lower pressure (20 psig) the smaller size group shows more potential for improvement than the larger one, because, as can be seen from Fig. 4-A.5, the efficiencies at this pressure are relatively small on a moistened surface.

This suggests that a zig-zag motion advancing laterally approximately 1/10 of the working width of a cleaning tool would be the technique to fully utilize the maximum removal capability of the concept. This does not necessarily mean that it is meaningful to do so. As we have seen earlier, nearly 100 percent removal could be achieved on a dry surface with one stroke only. In this case a repeated cleaning would not improve the situation but, in contrast, would only introduce recontamination hazards.

5. Entrainment. Flow tests were conducted with smoke injected upstream of the vacuum nozzle from various directions. Taft probes placed into the throat of the vacuum nozzle indicated that, at shallow angles below 40 degrees, and at pressures above 15 psig, the blow-jet would penetrate and reverse the vacuum flow at the far side of the vacuum nozzle. At steep angles above 50 degrees, the blow jet would fan out broadly and blow past the vacuum nozzle in all directions. Best conditions appeared to exist about a 45 degree angle.

To establish the amount of particulate matter detached but not removed, a second clean sample slide was placed underneath the test sample at a distance of 2 cm. In this poisition the sample slide restricting the flow into the vacuum nozzle should catch most of the particulates not entrained.

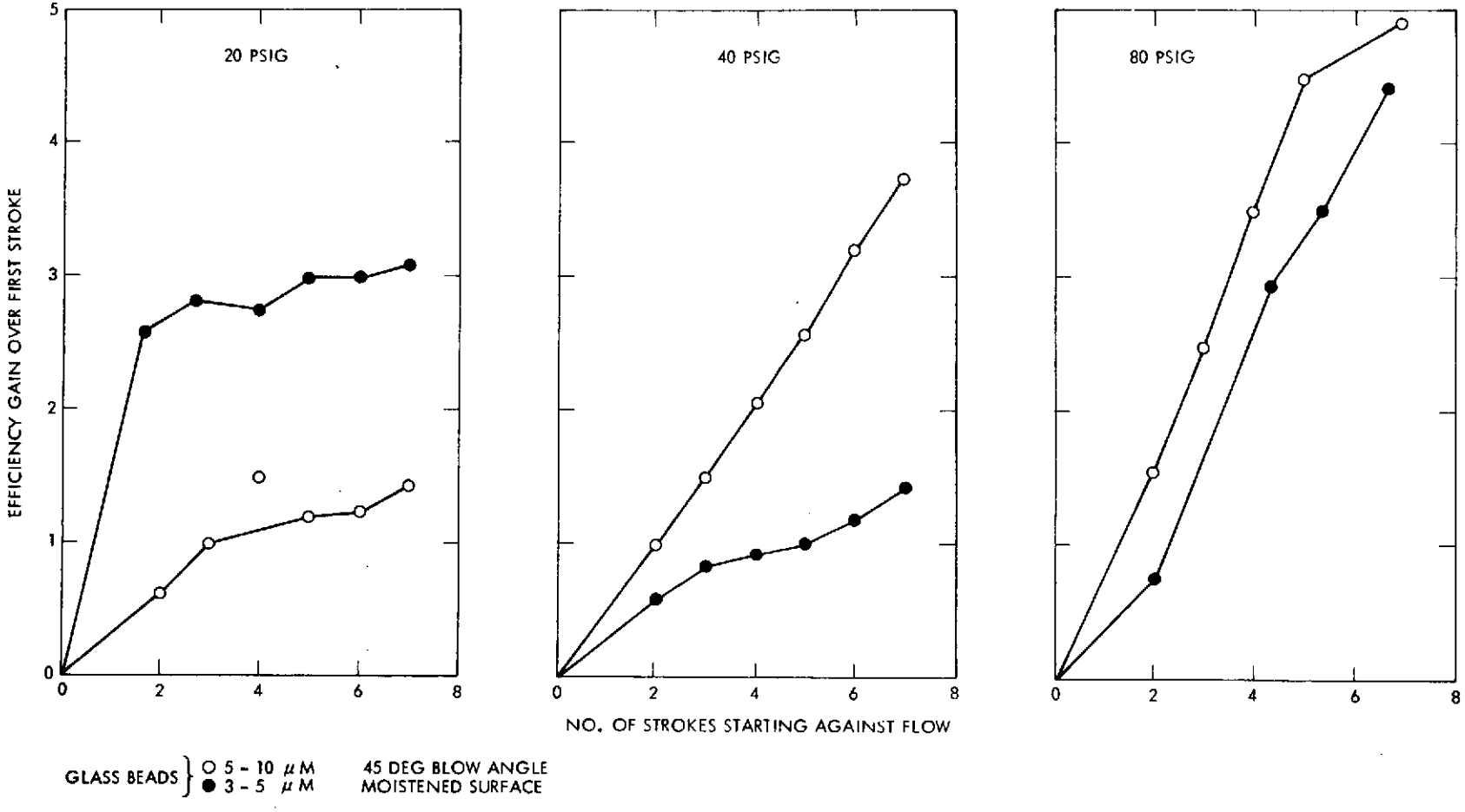

Fig. 4-A.7. Efficiency gain vs number of strokes

At all pressures tested, the largest amount of particles found on the lower slide was on the order of 3 percent of the particles removed from the test samples. This is a relatively small amount. With a slightly larger vacuum nozzle and with an opposite or circular arrangement of two or more blow nozzles, this possibly could be avoided.

4.1.3.2 Tests with Dust. Based upon the conclusions drawn from tests with glass beads, a 45 degree blow angle and a 1 cm sweep were chosen to conduct the tests. A separate sample was prepared for each of the pressures and surface conditions tested. Two determinations for each data point were made.

Various explanations have been advanced relative to the number and location of microorganisms attached to (or within) dust particles such as x viables per particle, y viables per unit of particle surface area, or z viables per unit of particle volume. Plotted in Fig. 4-A.8 are the total removal efficiencies achieved for dust particles (assumed to be homogenous in material. identical in size and shape, and the measured dimension $\geq 3\mu m$), in terms of three particle characteristics, quantity of particles, particle surface area, and particle volume. This information is useful in interpreting the potential biological cleaning capability of the considered methods for the three microbial particle attachment explanations. In Figs. 4-A.9, 4-A.10 and 4-A.11, the effect on sizes is presented in the form of histograms. The solid, the dashed, and the dotted lines represent the distribution in existence: prior to test; after sweeping with the vacuum nozzle only; and after blowing at the indicated pressure, respectively. The distributions are in terms of percent total original counts for all detectable particles $\geq 3\mu m$.

Comparing Fig. 4-A.8a with identical tests conducted with glass beads (Fig. 4-A.5), it can be seen that the relationship between the number of particles removed, the effect of blow pressures and surface conditions are essentially the same. As expected, the efficiencies achieved are lower than the ones obtained with glass beads. The pressure - efficiency relation, however, becomes different if we compare efficiencies in terms of surface area or volume removed (see Fig. 4-A.8, B and C). The reason for this is the fact that, in contrast to beads, the large dust particles (see Figs. 4-A.9, 4-A.10 and 4-A.11) are harder to remove than the smaller ones, particularly if the surface is oily or moist. At low (15 psig) blow pressures, some of the

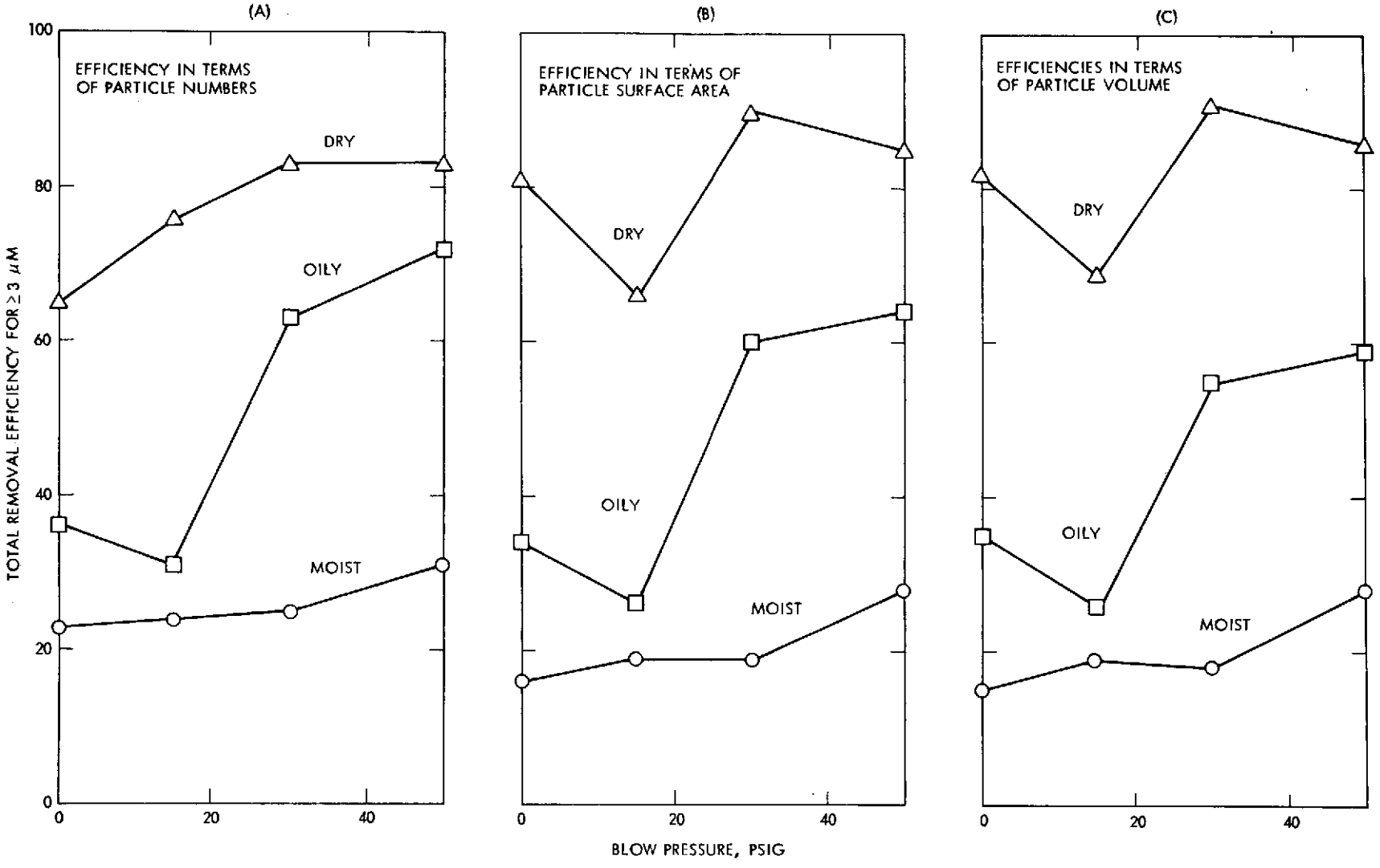

Fig. 4-A.8. Tests with dust – total removal efficiencies vs pressure and surface conditions (45 deg blow angle, double sweep)

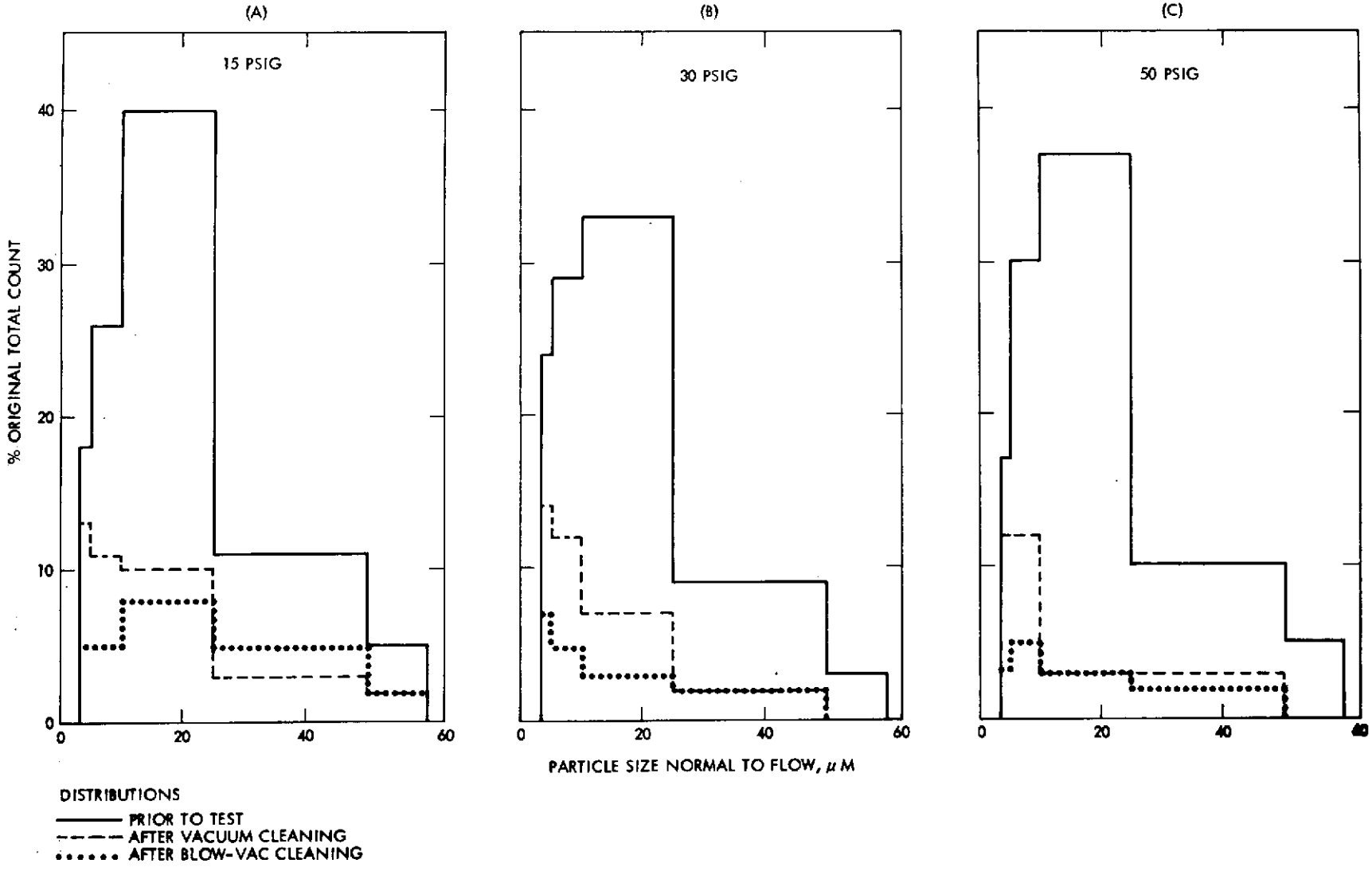

Fig. 4-A.9. Tests with dust on dry surface; effect on size (45 deg blow)

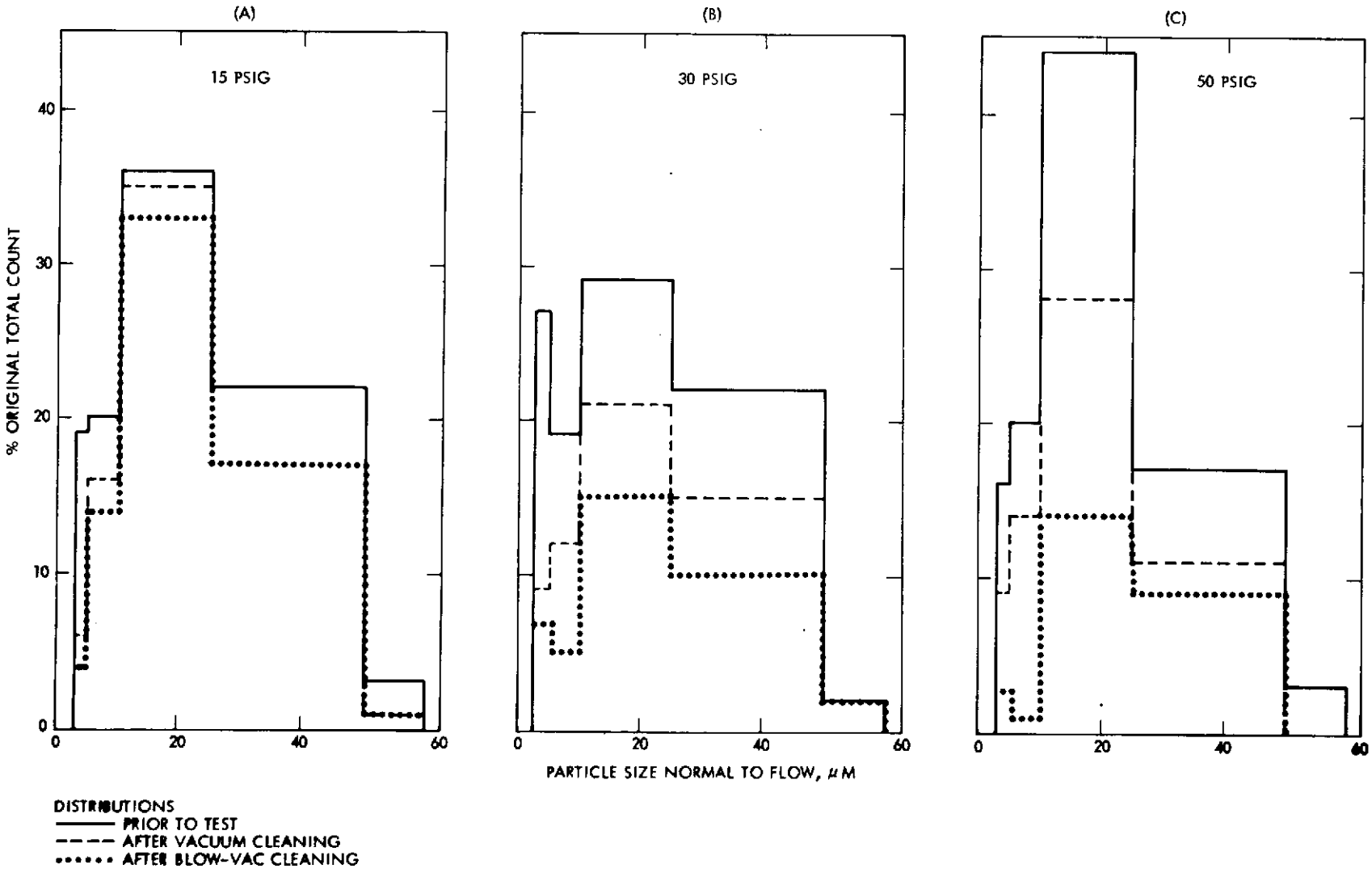

Fig. 4-A.10. Tests with dust on oily surface; effect on size (45 deg blow)

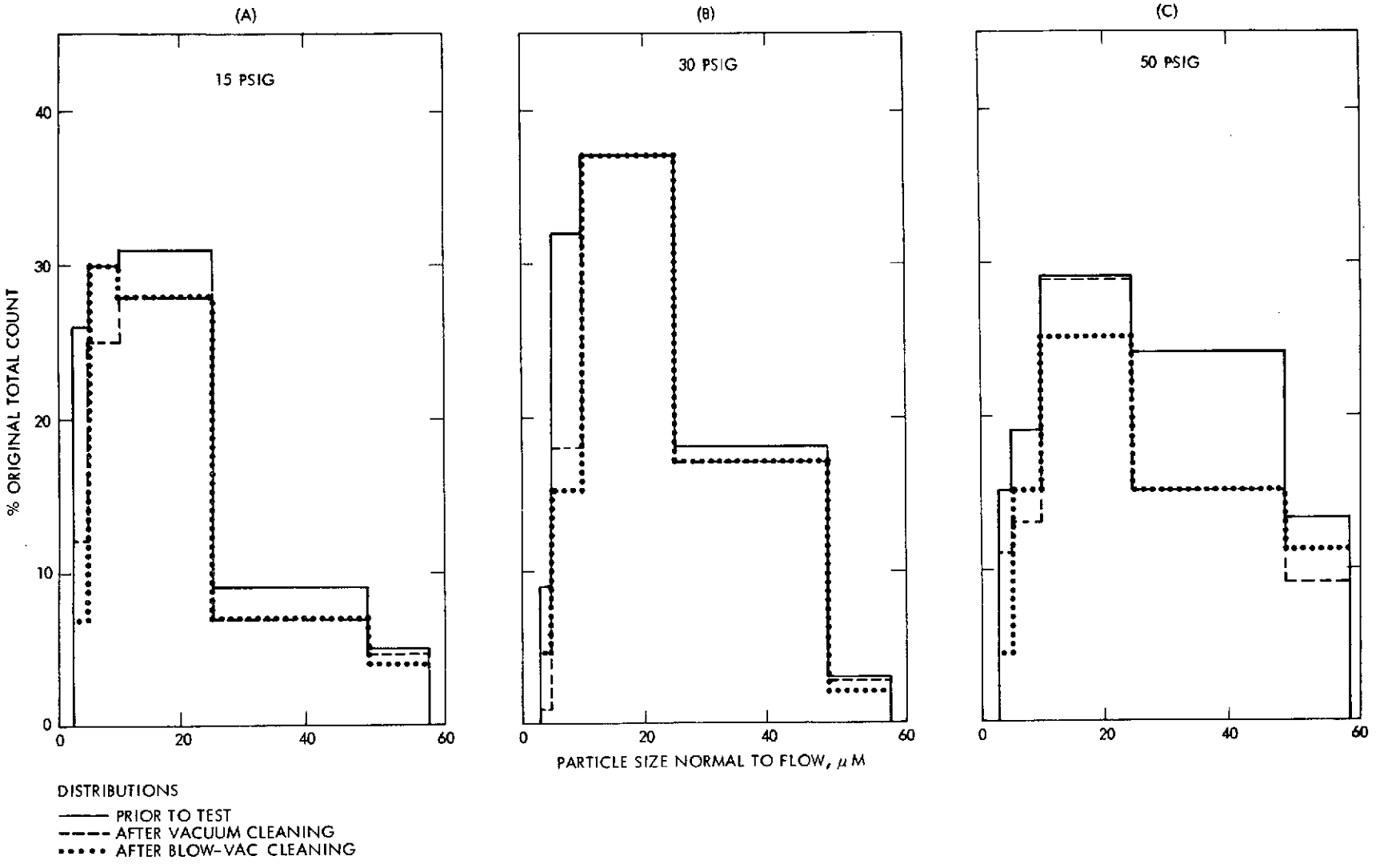

Fig. 4-A.11. Test with dust on moistened surface; effect on size (45 deg blow)

larger size particles tend to migrate into the reference area without being detached which, in Fig. 4-A.8 and B and C, shows up as a drop in efficiency, i.e., the blow has contaminated the reference area.

An explanation for this phenomenon is the heterogeneous composition of the dust particulates in terms of size, shape, and adhesive properties. For the dust collected it appeared that many of the particles larger than 10 μm were predominantly flat. Their contact area with the surface was relatively large in relation to their drag, when compared with glass beads of the same sizes. Many of the larger particles (> 30 μm) were fibrous in nature and, particularly on oil and moist surfaces, had the tendency to weathervane into the flow (and thus reduce drag).

4.1.4 Summary and Conclusions

In regard to the task objective, the discussed phase of the study concludes that:

1) Blow vacuum cleaning is a prospective method for the physical removal of particulate matter where the control of particulates between 5 and 50 μm sizes is of primary importance. Particles > 50 μm in size can be efficiently removed by vacuum flow alone. On particles ≧ 5 μm the method becomes very inefficient. The total removal efficiences demonstrated and believed feasible with a cleaning device that utilizes the described concept are summarized in Table 4-A.1. These data are based upon tests with dust.

Table 4-A.1. Blow vacuum cleaning test efficiencies demonstrated with dust seeded on optical glass (45 deg angle, double sweep)

Surface Conditions	Blow Pressure	Percent of Particulate Matter ≧ 3 μm Removed in Terms of:		
—	psig	Particle Numbers	Particle Surface Area	Particle Volume
Dry	30	85	90	90
Oily (fingerprinted)	50	70	65	60
Moist (fogged)	80	40	40	40

2) On normally dry surfaces (≥ 50 percent RH) pressures on the order of 30 psig across the blow nozzle are required to achieve a significant improvement over cleaning with vacuum flow alone. Blowing at lower pressures tends to induce particle migration without detachment, and is contaminating in nature. Pressures of 50 to 80 psig are required to efficiently remove particulate matter from oily surfaces and from surfaces that have been exposed to moisture condensation shortly before cleaning. Pressures on this order are usually compatible with solid surfaces. Blowing into entrapped areas, however, may result in pressure actions not compatible with the spacecraft design. A further reduction of the effective blow pressures is desirable to make the method more generally applicable.

3) A jet-angle on the order of 45 degrees against the surface should be a reasonable choice from the standpoint of efficiency and entrainment. Larger, i.e., steeper, blow angles appear to be more efficient on particles ≥ 5 μm (better penetration of sublayer) but entrainment becomes a problem that calls for a different conceptual approach. Thought should be given to this in further studies, if the removal of the smaller particulates is desired.

4) The continuous working speed should not exceed 0.5 cm/second unless the surface is oil-free and dry. Oscillating strokes advancing approximately 1/10 of the working width of the device in a lateral direction is probably the most practical working method from the time and efficiency standpoint. Strokes should start and end with an upstream sweep of the blow-jet to reduce recontamination hazards.

5) For uniformly shaped particles such as glass beads, the removal capability decreases with size and drops off sharply at sizes below 5 μm. For heterogenous particulate matter, such as dust, the removal of the larger particulates between 10 and (up to) 50 μm seems to represent more of a problem, if the removal of surface area and volume (rather than number) is the objective.

The presence of large numbers of flat and fibrous particles in this size range are primarily responsible for this phenomenon. Regardless of experimental problems and inconveniences associated with dust, more emphasis on test with dust must be given in further studies to draw final conclusions.

4.1.5 Future Activities

The objective of future activities is to reduce the blow pressures needed for efficient cleaning with flow, and to improve the capability for the removal of medium size dust particles (10-30 μm) from moist and oily surfaces. Since brushes will be used in certain areas, the effort will also concentrate on resolving the most pressing problems associated with brushes that have been identified in earlier tests.

4.1.5.1 Flow-Cleaning. The improvement for flow cleaning will go into the direction of utilizing pulse-effects to enhance particle detachment. Attachment to the existing apparatus will produce jet pulses up to approximately 22,000 Hz and focused harmonic pressure fluctuations up to 30,000 Hz. This will allow the study of the effect of blow-pressures, pulse frequency and intensity, on the removal capability of the blow jet. Glass beads and presized (Arizona road) dust seeded on optical glass will be used as test and sampling materials.

4.1.5.2 Brush Cleaning. The major problems to be resolved are those of (a) bristle materials, their mechanical properties and compatibility with decontamination and sterilization procedures, (b) accumulative contamination due to poor entrainment of the detached particles resulting from bristle packing and entanglement, and (c) the restoration of brush cleanliness during use.

The objective is to establish criteria for the selection of materials and design parameters for spacecraft cleaning brushes, and to devise the necessary methods to clean the brushes during use.

4.2 EVALUATION OF PLASMA CLEANING AND DECONTAMINATION TECHNIQUES

4.2.1 Subtask B Introduction

Heat and chemicals have been traditionally used as spacecraft microbial decontaminants. However, certain materials and complex equipment often suffer degradation and a loss in reliability due to heat damage or chemical incompatibility.

Plasma cleaning and sterilization involves exciting a gas and passing it over the material to be sterilized. The apparatus used includes a gas exciter (radio frequency), sterilization chamber and vacuum pump. In operation, specimens are placed in the sterilization chamber, pressure reduced, and excited gas is introduced. Sterilization is believed to occur although the parameters are not well understood, particularly as they may be applied to typical spacecraft applications. The plasma process does not appear to degrade materials which have been tested to date and, in addition, does not raise the temperature of the object being sterilized.

4.2.2 Significant Accomplishments

An 18 month contract was awarded to the Boeing Co. (May 15, 1973) to develop plasma sterilization technology for spacecraft application and generate preliminary design criteria for sterilizers. The study effort will be divided into two major areas: 1) define or determine the effective sterilizing ranges of different gases as a function of power, gas flow rate, and chamber pressure; 2) determine penetration characteristics and material compatibility of plasma and develop design criteria for plasma sterilizers.

4.2.3 Future Activities

Complete the contractual effort by October 15, 1974.